Durable Fast-charging Lithium Metal Batteries Designed with Cross-linked Polymer

**Electrolytes and Niobate-coated Cathode** 

Min-Huei Chiou a, Kristina Borzutzki a, Johannes Thienenkamp a, Marvin Mohrhardt a, Kun-

Ling Liu<sup>a</sup>, Valeriu Mereacre<sup>c</sup>, Joachim R. Binder<sup>c</sup>, Helmut Ehrenberg<sup>c</sup>, Martin Winter<sup>a,b</sup> and

Gunther Brunklaus a,b\*

<sup>a</sup> Forschungszentrum Jülich GmbH, Helmholtz-Institute Münster, IEK-12, Corrensstraße 46,

48149 Münster, Germany.

<sup>b</sup> MEET Battery Research Center / Institute of Physical Chemistry, University of Münster,

Corrensstrasse 46, 48149, Münster, Germany

<sup>c</sup> Karlsruhe Institute of Technology, Institute for Applied Materials, Hermann-von-Helmholtz-

Platz 1, 76344, Eggenstein-Leopoldshafen, Germany

\* PD Dr. G. Brunklaus,

Phone: +49 251 83-36756

Email: g.brunklaus@fz-juelich.de

Forschungszentrum Jülich GmbH, Helmholtz-Institute Münster, IEK-12, Corrensstraße 46,

48149 Münster, Germany.

**Abstract** 

A durable lithium metal polymer battery with extended cycle-life is designed by exploiting

cross-linked poly(trimethylene carbonate) (PTMC) electrolytes and LiNi<sub>0.6</sub>Mn<sub>0.2</sub>Co<sub>0.2</sub>O<sub>2</sub>

(NMC622) with well-defined protective coating (0.5 wt% of LiNbO<sub>3</sub> on the surface layer, <5

nm thickness). The presented materials demonstrate feasibility of faster cycling at rates of 1C

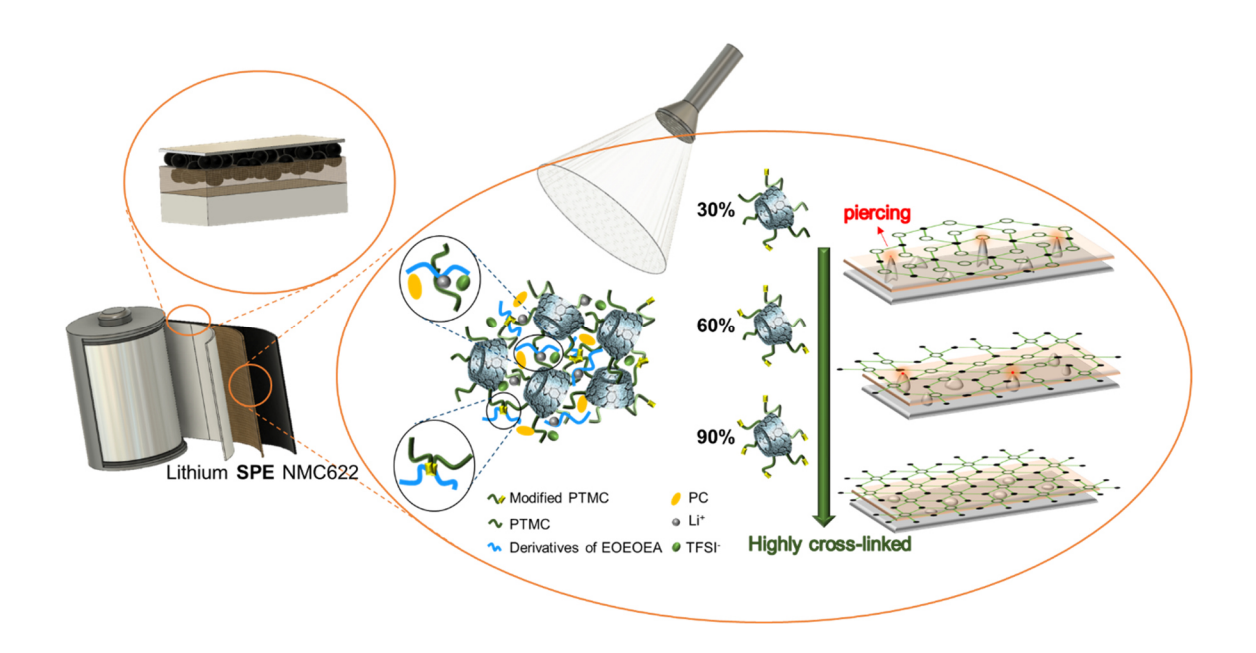
and 2C at temperatures of 40 and 60 °C, exhibiting prominent capacity retention of 91% and

80% SOH (state of health) after 500 cycles. At higher cross-linking densities, the introduced

quasi-solid polymer electrolytes afford good cycling performance and sufficient suppression of

high surface area lithium depositions as well as improved ability of solvent entrapment, hence

reflecting a considerable step forward towards achieving all solid-state polymer-based cells.



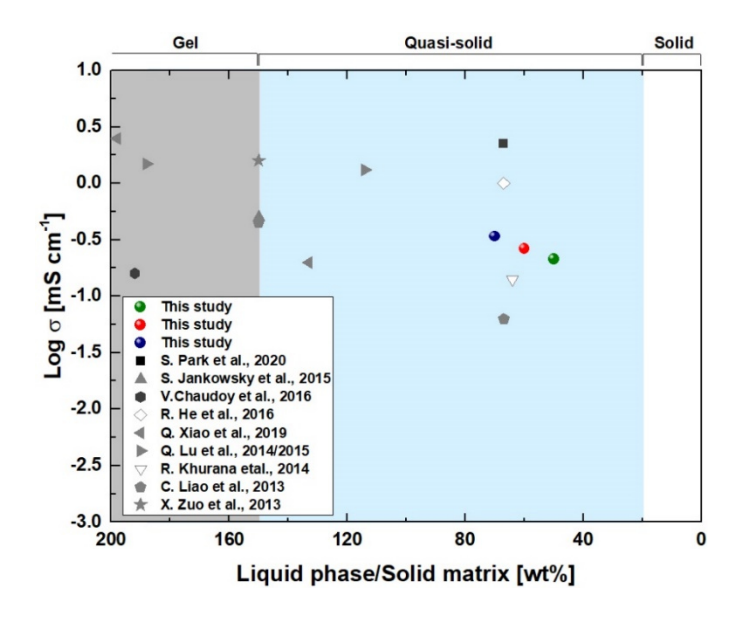
Keywords: cross-linked polymer, quasi-solid electrolyte, polycarbonate-based polymer electrolyte, grafted cyclodextrin, lithium metal battery, LiNbO<sub>3</sub> coated NMC622

# 1. Introduction

Lithium metal polymer batteries offer higher volumetric energy density and safer operation conditions compared to lithium ion batteries (LIB). Despite its high specific capacity (3860 mAh g<sup>-1</sup> and 2046 mAh cm<sup>-3</sup>), the application of lithium metal anodes is facing challenges including its tendency to form high surface area lithium (HSAL; often named after the post prominent morphology: "dendrites") upon fast charging. Polymer electrolytes (PEs) with compressive mechanical properties are considered beneficial to eventually mitigate inhomogeneous lithium deposition or the growth of HSAL fractions, [1-4] and in particular possessing mechanical moduli in the range of MPa may be sufficient to preferably obtain mossy lithium deposition during the operation of lithium metal batteries (LMBs). [5-8] All-solid "dry" polymer electrolytes, however, tend to have room temperature ionic conductivities below 0.1 mS cm<sup>-1</sup>, often limiting their applications to disadvantageous cycling rates (<0.5 C) and operational temperatures (≥60°C). [9, 10] Consequently, a plethora of polymer composites, gel

polymers and "quasi-solid" polymer electrolytes was introduced. [11-14] Among these, "quasisolid" polymer electrolytes that exhibit salient features, including mechanical flexibility for straightforward processing, good contacts to composite electrodes or even physical "entrapment" of plasticizers, constitute competitive candidates compared to currently available all-solid "dry" electrolytes. [15, 16] Notably, polymer-grafted cyclodextrins (GCDs) are prominent in the field of drug delivery, mainly due to their high bio-compatibility, [17, 18] but they are rarely adopted as battery electrolytes. Previous works of grafted polyrotaxanes (GPRs), functionalized derivatives of GCDs, however, disclosed the significant potential of GCD employment as solid polymer electrolyte (SPE), demonstrating effective lithium-ion pathways mainly along the grafted polymer side chains rather than inside the channels formed by the cyclodextrins, hence indicating that the backbone polymer onto which CDs are threaded is essentially not required to enhance the achievable ion transport. [19, 20] Besides, controlled synthesis of interlocked GPRs remains challenging due to the unavoidable issue of partial de-threading, [21, 22] leaving GCDs as an attractive alternative class of materials that can be designed with similarly beneficial features, except for insufficient mechanical properties in view of high surface area lithium (in particular dendrite and angular deposits) penetration. The latter can be strategically compensated by externally induced cross-linking. Though some studies have successfully evidenced cross-linking to strengthen resulting mechanical properties of target polymers, they are devoid of systematic elucidation of the impact of cross-linking densities and choice of constituents on the materials properties and cell performances.<sup>[23-25]</sup> Therefore, in the present mechanically elastic and structurally amorphous PTMC-based electrolytes straightforwardly derived from ring-opening polymerization (ROP) forming short polymer side chains (13-15 units of monomers on average) in the presence of  $\alpha$ -cyclodextrin ( $\alpha$ -CD) initiators (that in principle could afford 18 active sites in total) are explored. [26] The terminal functional groups of the PTMC polymer side chains were intendedly modified to varying degrees (ranging from 30%, 60% to 90%) and cross-linked in a mixture of 2-(2-ethoxyethoxy) ethyl acrylate

(EOEOEA) as comparable diluent,<sup>[27]</sup> lithium salt and propylene carbonate (PC), in this way establishing the impact of the cross-linking density on the ability of ideally irreversible solvent entrapment, resulting mechanical properties as well as achievable electrochemical performance of all the electrolytes operated in NMC622||Li cells.



Scheme 1. Overview of reported ionic conductivities of cross-linked polymer electrolytes, each operated with different amounts of plasticizer/solvent at room temperature. The composite cathodes contain NMC (dark gray, long-term cycling rate  $\leq$  0.2C) or LiFePO<sub>4</sub> (light gray, long-term cycling rate  $\leq$  0.5C). [24, 25, 28-35]

As displayed in **Scheme 1**, a number of cross-linked polymer electrolytes with liquid phases (plasticizer, solvent or molecular transporter),  $^{[36]}$  entrapped within the given polymer matrices either via chemical bonding or physical interactions, have been considered owing to their affordable skeleton structures and manufacture at industrial scales.  $^{[37,38]}$  Concerning the active materials of current cell designs, high performance Ni-rich cathodes (LiNi<sub>x</sub>Mn<sub>y</sub>Co<sub>z</sub>O<sub>2</sub>, x  $\geq$ 0.5) in principle could deliver higher energy density (160-210 mAh g<sup>-1</sup>) often requested by market demands for contemporary power supplies in e.g. electric vehicles, however, at the expense of complex surface chemistries that eventually result in oxidative decomposition of electrolyte constituents along with significant capacity losses even in case of polymer electrolytes.  $^{[39]}$  Therefore, a majority of current polymer electrolytes remains constrained to the application with lower energy density cathodes such as LiFePO<sub>4</sub>(LFP, 150-160 mAh g<sup>-1</sup>), mainly attributed

to its reasonably robust surface chemistry, narrower electrochemical operation window (with cutoff voltages <4.0 V) and high thermal stability, affording longer lifespan of corresponding cells. [28-32, 34, 35, 40] It should be noted that environmental concerns, natural abundance of any precursors, the demonstrated ability of LFP cathodes for fast charging (even at rates of up to 15C) as well as the possibility to get a better cell-to-pack volume ratio of cells using LFP, these days fuel renewed interest of world-wide automotive industry in the application of LFP-type cathodes. In cases where NMC-based cathodes are indispensable, exploitation of coatings or protective layers on cathode active materials to mitigate detrimental side reactions occurring between the cathode surface and electrolyte components represents a valid concept to foster prolonged cycling life of cells. For this reason, several coating materials, including Al<sub>2</sub>O<sub>3</sub>, SiO<sub>2</sub>, TiO<sub>2</sub>, ZrO<sub>2</sub>, WO<sub>3</sub>, and especially LiNbO<sub>3</sub>, were elucidated in the presence of liquid or solidstate electrolytes (SSEs).[41-46] Herein, high energy density lithium metal polymer batteries with NMC622 cathodes and GCD-based polymer (PTMC) electrolytes are introduced to afford longterm (>500 cycles) rapid charge/discharge at moderate temperatures of 40 °C (1C) and 60 °C (2C), which are not presented yet in the other studies of cross-linked polymers in quasi-solid systems (mostly ≤0.5C, see in **Scheme 1**). Notably, the otherwise often observed capacity fading could be remarkably reduced by systematically tuning the actually achieved degree of cross-linking in this class of materials, exhibiting robust cycling performance at rates of 1C over 500 cycles at 91 % capacity retention. In addition, "planar" morphology of lithium deposits could be identified, illustrating enhanced reversibility to exploit the available lithium reservoir in NMC622||Li cells operated with suitably tailored "quasi-solid" polymer electrolytes.

# 2. Experimental

#### 2.1. Material

α Cyclodextrin (98%, further dried under vacuum at 80 °C for 2 days) and 1,3-Dioxan-2-one (98%) were received from abcr GmbH. Benzoic acid (≥99.5%), 1,8-Diazabicyclo [5.4.0] undec-

7-ene (DBU), mono-Ethyl fumarate (FAME, 95%), N,N'-Dicyclohexylcarbodiimide (DCC, 99%), 4-(Dimethylamino)pyridine (DMAP, ≥99%), 2,2-Dimethoxy-2-phenylacetophenone (DMPA, 99%), 2-(2-Ethoxyethoxy) ethyl acrylate (EOEOEA, dried over 4 Å molecular sieves), Dimethyl sulfoxide (DMSO, ≥99.9%, dried over 4 Å molecular sieves to reduce water contents to ≤20 ppm), Dimethyl sulfoxide-d<sub>6</sub>, Methanol (≥99.9%), Dichloromethane (anhydrous, ≥99.8%), Chloroform (anhydrous, ≥99%), N-methyl-2-pyrrolidone (NMP, anhydrous, 99.8%) and Petroleum ether were purchased from Sigma Aldrich, Germany. NMC622 and propylene carbonate (PC) were bought from BASF. Lithium bis-trifluoro-methane-sulfonimide (LiTFSI), carbon black and polyvinylidene difluoride (PVDF) were obtained from Solvionic, Imerys and Solvay, Belgium, respectively.

# 2.2. Synthesis of PTMC-grafted CDs and end-group modification

0.19 g of  $\alpha$  Cyclodextrin (0.20 mmol) was dissolved into 10 ml anhydrous DMSO, followed by dropping 0.18 g of DBU (5.99 eq., 1.17 mmol) as a catalyst to deprotonate the hydroxyl groups on cyclodextrin. After stirring for 30 minutes, 3.00 g of 1,3-Dioxan-2-one (150.82 eq., 29.41 mmol) dissolved in 8 ml DMSO was slowly added in. The reaction took place at 60 °C with argon purging for 24 h. Afterwards, the solution was cooled down and 0.40 g of benzoic acid (16.82 eq., 3.28 mmol) was added to terminate the reaction. The product was then precipitated from methanol (5 ml of solution into 35 ml of methanol) at 15 °C and collected by centrifugation. After being dried for 24 h under vacuum (10<sup>-3</sup> mbar) at 60 °C and another day under vacuum (10<sup>-6</sup> mbar) at 40 °C, a yellow-brownish rubbery polymer was obtained with an overall yield of 70%. The molecular identity of PTMC-grafted CDs (**Figure 1**) was confirmed by <sup>1</sup>H NMR spectroscopy (Table S1 and Figure S1a, Supporting Information), and the molecular weight was calculated as 11k (Mn 8.9k and PDI 2.2 from GPC shown in Figure S2, Supporting Information).

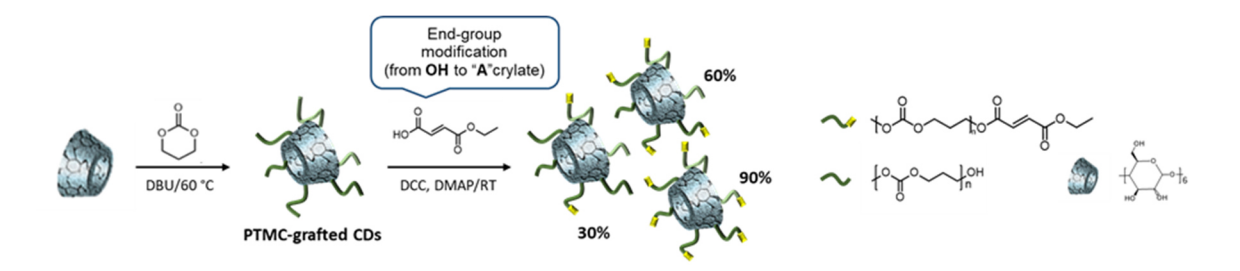


**Figure 1.** Schematic representation of the required steps for synthesis of PTMC-grafted CDs, comprising reaction of CDs with the cyclic monomers and end-group modification with acrylates.

2.20 g of PTMC-grafted CDs (Mn 11k from NMR, 0.20 mmol) was dissolved into 8 ml anhydrous dichloromethane together with 0.08 (0.16, 0.24) g of FAME (2.75 (5.50, 8.25) eq., 0.55 (1.10, 1.65) mmol) and mixed for 30 minutes. A solution containing 0.11 (0.22, 0.33) g of the coupling agent DCC (2.75 (5.50, 8.25) eq., 0.55 (1.10, 1.65) mmol) and 0.01 g of the catalyst DMAP (0.50 eq., 0.10 mmol) in 0.80 ml anhydrous chloroform were subsequently added dropwise. The reaction occurred at room temperature (RT) under argon atmosphere and was continued for 48 h (in **Figure 1**).<sup>[47]</sup> After that, the white salt (dicyclohexylurea) generated during the reaction and insoluble in dichloromethane was removed by filtration, and the product was precipitated from petroleum ether at 15 °C, followed by the same drying process as PTMC-grafted CDs. Finally, a white-brownish rubber-type polymer was received with a yield of 86% (~1.96 g). The ratio of modified groups where cross-linking was managed to be proceeded over all of terminal functional groups had been confirmed by <sup>1</sup>H NMR spectroscopy with 30%, 60% and 90% modification (Table S1 and Figure S1, Supporting Information). Small group substitution has minor effects to the overall molecular weight of polymer, corroborated by GPC data showing Mn ~10k for each modified polymer (Figure S2, Supporting Information).

## 2.3. Preparation of polymer electrolyte membrane

Self-standing polymer membranes were prepared by blending modified PTMC based polymer (30%, 60% and 90% modification) with diluent EOEOEA (polymer:EOEOEA ratio of 3:1), 1-

2 wt% of initiator DMPA, preferable plasticizer PC (20-90% uptake, selection of plasticizer is presented in Figure S3a-c, Supporting Information) and optimized amount of LiTFSI ([C=O]<sub>polymers+plasticizers</sub>:[Li<sup>+</sup>] = 8:1, ~24 wt%, Figure S3d, Supporting Information). The viscous precursors were placed within two mylar foils with a gap of 150 μm and photo cross-linked after standing still overnight at RT for degassing. Thickness of 80 μm is feasible, though the difficulty of handling slightly enhances. The curing process lasted for at least an hour in an UVACUBE 100 to complete the reaction (Figure S4, Supporting Information). Herein, the resulting electrolyte membranes are referred as nA\_mPC, where "n" denotes the level of cross-linking density with 1, 2 and 3 corresponding to 30%, 60% and 90% modification, while "m" indicates the ratio of plasticizer amount to the "dry content" (polymer and Li salt), e.g. 1A 50PC.

$$m = \frac{W_{plasticizer}}{W_{dry\ content\ (polymer\ +\ lithium\ salt)}} \times 100\ \% \tag{1}$$

## 2.4. Preparation of cathode LiNi<sub>0.6</sub>Mn<sub>0.2</sub>Co<sub>0.2</sub>O<sub>2</sub> (NMC622)

0.5 wt% LiNbO<sub>3</sub> (thickness of few nanometers, <5 nm) coating on NMC622 (BASF) was applied by a method of chemically activated coating. The Li/Nb coating solution and coated NMC622 particles were prepared using a method similar to that described in available literature. [44] Two solutions were prepared: 0.057 g (1.10 mmol) LiOC<sub>2</sub>H<sub>5</sub> was dissolved in 40 ml anhydrous (absolute) ethanol. Separately, 0.301 g (0.95 mmol) Nb(OC<sub>2</sub>H<sub>5</sub>)<sub>5</sub> was dissolved in 20 ml anhydrous (absolute) ethanol. Under magnetic stirring of the first solution, the second one was added. To obtained the mixture, 60 ml of H<sub>2</sub>O<sub>2</sub> (30%) was further introduced, and the resulting Li/Nb coating solution was stirred for additional 10 minutes. Subsequently, 103 ml Li/Nb coating solution was added in a round bottom flask (2000 ml) containing 24 g NMC622 (BASF) and 220 ml anhydrous (absolute) ethanol under stirring. After two hours of stirring, the reaction mixture was decanted and the obtained powder washed with 100 ml anhydrous

(absolute) ethanol, and dried for one hour at 100 °C. The obtained dry powder was calcined as previously reported.<sup>[48]</sup>

1.00 g (90 wt%) of active material (NMC622 from BASF and 0.5 wt% LiNbO<sub>3</sub> coated NMC622 from KIT) was blended with 0.03 g (3 wt%) PVDF binder, 0.08 g (7 wt%) conductive carbon and 2 ml NMP solvent in a Thinky mixer for 10 min at 1700 rpm speed. Subsequently, the cathode slurry was cast onto Al foil, where surface contamination was removed by ethanol treatment, employing a doctor blade technique with a 50  $\mu$ m gap width. Afterwards, the obtained sheet was dried at 80 °C overnight to remove residual solvent and then roll pressed to 37  $\mu$ m, including 20  $\mu$ m of Al foil (mass loading of 2.5 mg cm<sup>-2</sup>). Finally, the electrode was punched and further dried under vacuum ( $10^{-3} \text{ mbar}$ ) at 120 °C for one day and vacuum ( $10^{-6} \text{ mbar}$ ) at 110 °C for another day.

#### 2.5. Cell assembly

A common sandwich method where the bubble-less polymer membrane (thickness of 130-150 μm, diameter of 12 mm) was placed in the middle of a mylar foil ring (diameters of 16 mm and 13 mm for outer and inner) between two electrodes in a CR2032 coin-cell configuration was used. Lithium metal foil was roll-pressed from 500 μm to 300 μm (diameter 14 mm), and two NMC622 cathodes (diameter 10 mm) with and without 0.5 wt% LiNbO<sub>3</sub> coating (cathode mass loading: 2.5 mg cm<sup>-2</sup>) were used for comparison. The process was performed in a dry room with a dew point <-66 °C.

#### 2.6. Material characterization

#### 2.6.1 <sup>1</sup>H nuclear magnetic resonance

<sup>1</sup>H NMR spectra were recorded at a BRUKER 400 AVANCE III HD spectrometer using deuterated dimethyl sulfoxide (DMSO-d<sub>6</sub> that appears at 2.5 ppm) as reference signal for <sup>1</sup>H spectra.

# 2.6.2 Gel permeation chromatography

The GPC system was an Agilent 1260 Infinity instrument equipped with PolyPore columns and an RI detector. The mobile phase was Dimethylacetamide (DMAc). Poly(methyl methacrylate) (PMMA, ReadyCal-Kits) standards in the range of 0.8-2200 KDa were used to calibrate the system with flow rate of 1.0 ml min<sup>-1</sup> at 23 °C (R >0.99).

## 2.6.3 Rheology

Mechanical properties of polymer membranes were measured by a modular compact rheometer (MCR102) from Anton Paar with a measuring system of PP15-SN71066 (diameter of 15 mm). Amplitude ( $\gamma$ ) was set to a constant value of 0.5%, and angular frequency varied in the range of 200 to 1 while a normal force was fixed at 1 N.

#### 2.6.4 Raman spectroscopy

Raman measurements were conducted with a SENTERRA Bruker microscope spectrometer under 50× Raman at RT, applying a laser source at 785 nm with a power of 25 mW. The spectral resolution was 9-15 cm<sup>-1</sup> in the wavenumber range from 75 cm<sup>-1</sup> to 3200 cm<sup>-1</sup>.

#### 2.6.5 Scanning electron microscopy

SEM was utilized to determine the lithium surface morphologies and lithium deposits on the polymer membranes. Multiple areas of each sample were analyzed at an Auriga CrossBeam workstation from Carl Zeiss (Germany), exploiting an acceleration voltage of 3 kV.

# 2.6.6 Pulsed field gradient nuclear magnetic resonance

All the NMR spectra were recorded with a  $B_{RUKER}$  4.7 T AVANCE III instrument equipped with a commercially available  $B_{RUKER}$  Diff50 probe. Pulsed field gradient nuclear magnetic resonance (PFG-NMR) data were acquired with a (doubly tuned  $^7\text{Li}$  &  $^1\text{H}/^{19}\text{F}$ ) 5 mm coil at 40 °C (±0.2 °C). A 0.25M LiCl in H<sub>2</sub>O solution and a 3M KF in H<sub>2</sub>O solution were utilized for external calibration. Max. gradient strength of 16 gradient steps was set to 2947 G/cm averaging up to 16 scans with a gradient pulse length  $\delta$  of 1 ms and diffusion time  $\Delta$  of 40 ms. The corresponding

 $^{19}$ F and  $^{7}$ Li self-diffusion coefficients D of the species were derived from a stimulated echo sequence (Bruker "diffSte") after fitting the attenuated signal amplitudes (integration) to the Stejskal-Tanner equation, which describes the case of isotropic diffusion

$$I = I_0 \times exp\left(-D\gamma^2\delta^2g^2\left(\Delta - \frac{\delta}{3}\right)\right) \tag{2}$$

with I being the signal intensity,  $I_0$  the initial signal in the absence of a magnetic field gradient and  $\gamma$  the gyromagnetic ratio.<sup>[49, 50]</sup> Data analysis was performed with Bruker Topspin 3.5 software and the Bruker Dynamics Center 2.5 program package.

An average degree of salt dissociation  $\alpha$  can be also estimated via the obtained self-diffusion coefficients with the Nernst–Einstein equation

$$\Lambda_e = \frac{\sigma}{c} = \frac{z_i^2 F^2}{RT} (D_+ + D_-)$$
 (3)

$$\alpha = \frac{\sigma_{imp}}{\sigma_{NMR}} \tag{4}$$

where  $\Lambda_e(\mathrm{Sm}^2/\mathrm{mol})$  refers to molar conductivity, c and  $z_i$  are the molar concentration and charge of ion species, respectively.<sup>[51]</sup>

# 2.6.7 <sup>7</sup>Li solid-state nuclear magnetic resonance

Anode-free cells were carefully disassembled from the coin-cell configuration (diameter of electrodes: 8 mm, polymer: 10 mm) after cycling (open circuit voltage: ~3 V) and sealed in pouch bags. Static <sup>7</sup>Li NMR experiments were performed at room temperature with an AVANCE III 200 MHz spectrometer operating at a magnetic field of 4.7 T leading to a Larmor frequency of 77.9 MHz for <sup>7</sup>Li. Spectra were recorded with a saturation recovery pulse length of 2.66 μs, a relaxation delay of 1 s and 1024 scans for each spectrum. The NMR spectra were referenced with respect to 1M LiCl solution (<sup>7</sup>Li, 0 ppm). Data analysis was performed with B<sub>RUKER</sub> Topspin 3.5 software applying automatic phase correction. Total intensity of the Li

metal was integrated over a shift range from 185 to 330 ppm, fitted with three distinct lithium metal peaks using a home-written MATLAB script.

#### 2.7. Electrochemical characterizations

#### 2.7.1 *Ionic conductivity*

The polymer membrane was punched to a 12 mm diameter disk (thickness of 130-180  $\mu$ m) and assembled in a coin cell (CR2032) between two stainless steel electrodes. Electrochemical impedance spectroscopy (EIS) was conducted using an Autolab device in the temperature range of 0 °C to 70 °C with 10 °C per step over a frequency range from 1 Hz to 1 MHz with a 10 mV sinus amplitude after preheating step scanning (20 °C to 70 °C).

#### 2.7.2 Transference number

The Li transference number was measured in a symmetric cell against lithium metal at 40 °C by Autolab PGSTAT302N (Metrohm, Modul: FRA V2.0, Nova-Software 2.1) after one-day equilibrium at 40 °C. A DC polarization voltage ( $\Delta V$ ) of 10 mV was applied for the potentiostatic polarization. The resulting current was recorded by time. Initial current indicates the condition when the ions can still move freely, and steady-state current reflects net flux of cation. The impedance spectra were collected between 1 Hz and 1 MHz before and after polarization. An equation of evaluating  $t_+$  built on an assumption of neglected ion-ion interaction proposed by Watanabe et al. was applied when the complex impedance spectra did not greatly change after polarization as following, [52-55]

$$t_{+} = \frac{R_b}{(V/I_{\infty} - R_e)} \tag{5}$$

where  $R_b$  and  $R_e$  refer to bulk and interfacial/interphasial resistance before polarization, respectively. PFG-NMR data and the corresponding self-diffusion coefficients of the ions also enable to establish transport numbers based on the Nernst-Einstein equation expressed as

$$t_{+} = \frac{Z_{+}D_{+}}{Z_{+}D_{+} - Z_{-}D_{-}} \tag{6}$$

where D denotes the ion self-diffusion coefficient, and Z is the ion charge.<sup>[56]</sup>

## 2.7.3 Electrochemical stability window

Linear sweep voltammetry (LSV) was executed by a patented device with three probes in a sealed holder to determine the electrochemical stability window at 60 °C using Autolab. [57] The sample was stuck at the bottom of the probe with thickness of 1 cm while measuring (Figure S5, Supporting Information). For oxidative stability, a three electrode configuration with the probe with lithium metal as a reference electrode, platinum as a working electrode and stainless steel as a counter electrode was used. [58] For reductive stability, the working electrode was changed to copper. The scan rate was controlled at 0.5 mV s<sup>-1</sup> and the potential scan range was up to 6.5 V vs. Li|Li<sup>+</sup> from open circuit potential (OCP) and down to -0.5 V vs. Li|Li<sup>+</sup> from OCP. Moreover, Galvanostatic approach against NMC622 in a coin cell (NMC622||Li) with 0.1C charge rate at 60 °C (cut-off voltage: 5 V; cut-off time: 30 h) was further applied to compare the results from LSV on platinum.

#### 2.7.4 Limiting current density

The limiting current density of an electrolyte was determined in a lithium symmetric coin cell where the polymer electrolyte laid in between of two lithium electrodes. The cell was equilibrated at a fixed temperature either at 20 °C, 40 °C or 60 °C for 12 h prior to the measurement, which was performed at a sweep rate of 0.02 mV s<sup>-1</sup> with a recorded current response on a Biologic VMP device.

# 2.7.5 Cell cycling condition

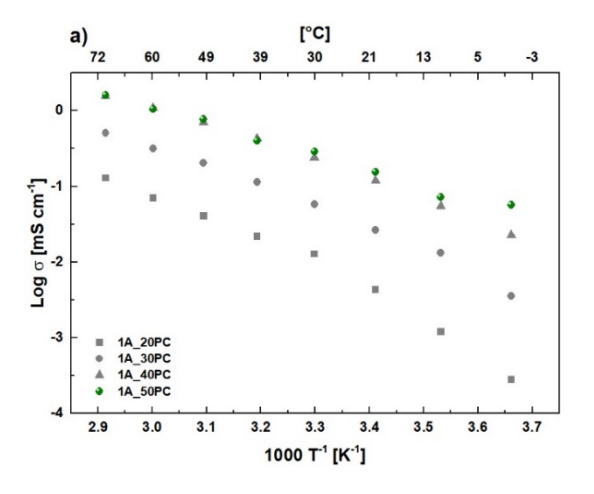
The stability of the electrolyte against lithium metal was measured by lithium stripping/plating in a symmetric lithium cell cycling with a current density of 0.1 mA cm<sup>-2</sup> (1 h per half cycle) as well as single-side plating with 0.2 mA cm<sup>-2</sup> current density for 10 h at 20 °C on Maccor

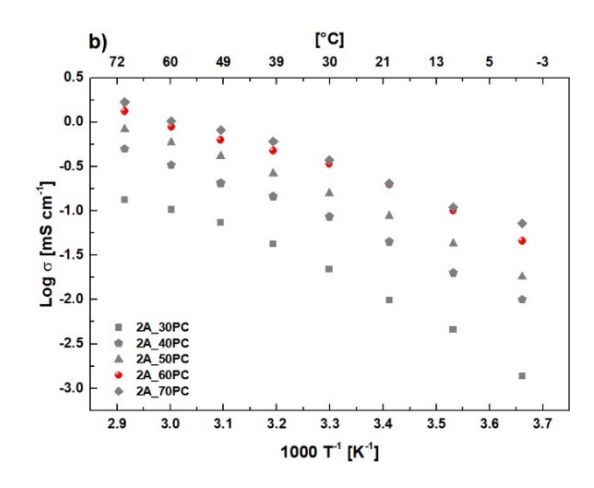
4000 battery analysis system (USA). An asymmetric full LMB cell (NMC622||Li) was cycled within a voltage range between 4.3 V and 3 V (constant current, theoretical specific capacity of 180 mAh  $\rm g^{-1}$ ) at 20 °C, 40 °C and 60 °C.

#### 3. Results and discussion

## 3.1. Ionic conductivity and solvent entrapment

Ionic conductivity, an essential electrochemical feature, is determined by the motion of charge carriers within the material's structure and often utilized as an initial criterion to appraise the usability of the considered electrolytes.<sup>[59]</sup> In view of lithium metal battery application, PTMC-based materials require the addition of a controlled dose of electrochemically robust plasticizers to boost the achievable ionic conductivities, though unlike common gel polymers, "physical" entrapment due to tailored degrees of cross-linking affords "quasi-solid" polymer electrolytes. The corresponding relations of plasticizer (PC) amounts and observed ionic conductivities of PTMC-based electrolytes with different cross-linking densities (1A, 2A and 3A) are displayed in **Figure 2**a-c.





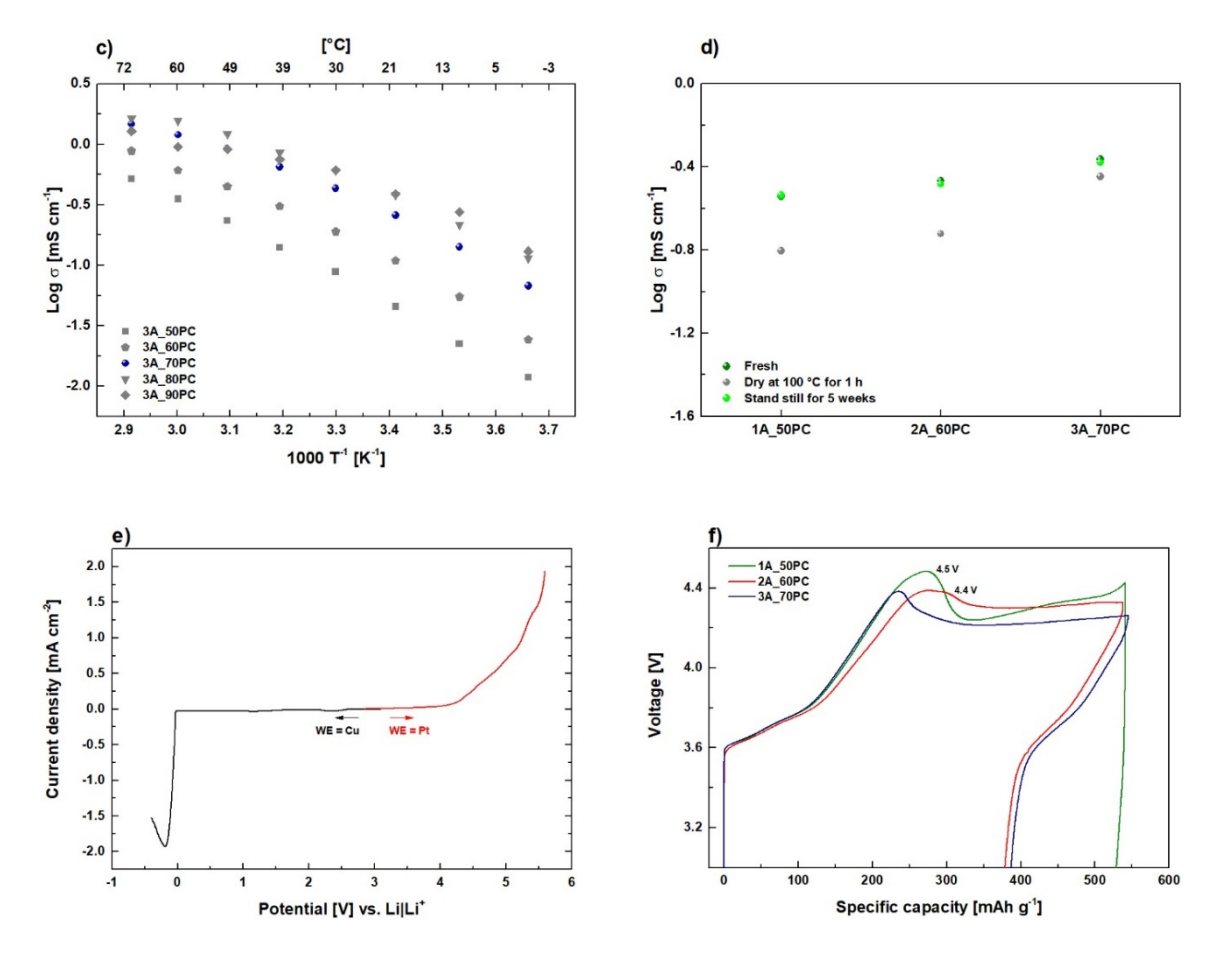


**Figure 2.** Overall ionic conductivities of cross-linked polymers: a) 1A in presence of various amounts of PC (20-50% uptake), b) 2A and c) 3A with 30-70% and 50-90% PC uptake, respectively. d) Ionic conductivities at 30 °C after drying, including resting in a dry-room for 5 weeks and thermal shock treatment at 100 °C for 1 h. e) ESW of 3A\_70PC obtained from potentiodynamic scans against inert electrodes at 60 °C; f) Galvanostatic charge of 1A\_50PC, 2A\_60PC and 3A\_70PC towards practical electrodes (NMC622||Li) with a rate of 0.1C at 60 °C.

A control of the cross-linking density dissimilar to the conventional approaches based on variable amounts of cross-linkers and molecular weights of monomers/oligomers (shown in **Scheme 1**) is achieved by adjusting the actual degree (30%, 60% and 90%) of end-group modification of PTMC-grafted CDs, in this way producing an anticipated copolymer network in the presence of 2-(2-ethoxyethoxy) ethyl acrylate (EOEOEA), which functions as a diluent in the mixed precursor and benefits membrane processing (e.g. less viscous rheology, less bubbles generated). [23, 60] As conjectured, the ion mobility is reduced within a strictly fastened structure of polymer matrix, and thus higher amounts of PC are involved to deliver similar degrees of ion transport in materials with higher cross-linking densities. In view of threshold

features of electrolytes (e.g. as suggested by the U.S. Advanced Battery Consortium) relevant for potential industrial applications, such as ionic conductivity of  $\sigma_{Li}^+ > 0.1$  mS cm<sup>-1</sup> for solid electrolytes, [61] the introduced quasi-solid electrolytes of 1A\_50PC, 2A\_60PC and 3A\_70PC provide reasonable overall ionic conductivities of ~0.3 mS cm<sup>-1</sup> at 30 °C (taking t<sub>+</sub> of 0.3-0.4 for PC as the reference) and achieve the threshold requirement, [62, 63] though at the expense of limited amounts of added plasticizers (PC quantity remains as low as possible). Since gel-type polymers or liquid electrolyte formulations containing propylene carbonate (PC) might be prone to safety issues such as fire or explosive risks, drying procedures were done to evaluate if the plasticizer is sufficiently entrapped within the polymer structures, avoiding leakage or other negative impact on the actual cell performance over the cell lifetime. In particular, after a duration of 5 weeks resting the materials in a dry room, a non-insignificant variation (less than 3.5%) of the ionic conductivities of each electrolyte could be identified, hence indicating nearly full retention of PC within the introduced polymer membranes, maintaining comparable qualities of "dried" and pristine materials (Figure 2d). If the polymer membranes are exposed to a thermal shock at 100 °C for one hour to mimic harsher environmental conditions, the ionic conductivities of the polymers are reduced due to partial losses of the plasticizers, especially in case of membranes with lower cross-linking densities (e.g. 45% and 44% conductivity reduction for 1A 50PC and 2A 60PC, reflecting a loss of ~5 wt% PC). By contrast, upon enhancement of the cross-linking density (30% to 90% modification) to strengthen the polymer framework but also improve the ability of solvent entrapment, merely losses of up to ~1.5 wt% PC could be observed, retaining reasonably ionic conductivity (3A 70PC: 17.5% conductivity reduction) after the thermal treatment.

#### 3.2. Transference number and cation solvation

Concentration polarization is a major impact factor to eventually induce HSAL formation due to inhomogeneous lithium deposition, rendering the overall current fraction provided by Li<sup>+</sup> ion transport highly important.<sup>[5]</sup> As shown in **Table 1**, the transference numbers of the introduced materials, as derived from potentiostatic polarization, amount to  $t_+ \le 0.3$  (also see Figure S6 and Table S2, Supporting Information) comparable to the reference polymer electrolyte of crosslinked polyethylene oxide (PEO), and other carbonate based liquid electrolytes.<sup>[62, 63]</sup> An alternative technique to evaluate molecular transport within electrolytes includes pulsed field gradient NMR, providing self-diffusion coefficients of both anions (<sup>19</sup>F) and cations (<sup>7</sup>Li) in the absence of electric fields (e.g. no current flow or voltage applied). The values reveal that ion transport numbers of  $\approx 0.3$  are in quite good agreement with data derived from electrochemical methods, indicating less impact from ion-ion interactions within the PTMC-based electrolytes (displayed in **Table 1**). Straightforward analysis of PFG data typically assumes complete ion dissociation and the absence of mobile ion pairs, ignoring ion-ion interactions, <sup>[52-55]</sup> so that a deviation of electrochemical and NMR data could be significant in cases where the presence of ion interactions and contributions from strongly correlated ion transport cannot be neglected.

**Table 1.** Transference and transport numbers measured from potentiostatic polarization and <sup>7</sup>Li, <sup>19</sup>F PFG-NMR at 40 °C, respectively. Degrees of salt dissociation obtained from self-diffusion coefficients and analysis of Raman shifts of TFSI anions within the polymer membranes.

40 °C	1A_50PC	2A_60PC	3A_70PC
<i>t</i> +	0.24±0.02	0.26±0.02	0.28±0.02
<i>t</i> + (PFG-NMR)	0.29	0.29	0.29
$D_{\text{Li}^+} (10^{-12} \text{ m}^2 \text{S}^{-1})$	2.69	4.19	5.69
$D_{\text{TFSi}}^{-}$ (10 <sup>-12</sup> m <sup>2</sup> S <sup>-1</sup> )	6.61	10.24	13.92
$\alpha_{(PFG\text{-}NMR)}$	89%	87%	87%
α(Raman), RT	83%	86%	80%

The actual degree of ion dissociation ( $\alpha$ ) of the considered electrolytes allows for an estimation of the presence of ion pairs; an average value of  $\alpha$  may be derived from NMR self-diffusion coefficients or Raman shifts (**Table 1**), e.g. TFSI signals; note that Raman data also afford comprehensive insight to the actually present ion coordination within electrolytes (see Figure S7, Supporting Information). Based on peak assignment of the corresponding Raman spectra that illustrate a combination of "free" TFSI anions (~740 cm<sup>-1</sup>) and TFSI anions included in contact ion pairs (~744 cm<sup>-1</sup>) as well as calculation of self-diffusion coefficients, [64, 65] all PTMC-based electrolytes exhibit remarkably higher degrees of ion dissociation (>80%) compared to literature-reported 1M (LiTFSI) PC electrolytes (e.g. 0.3 or 0.46)[51, 66, 67], reflecting the presence of merely minor ion interactions in these systems, likely attributed to polymer oxygen (e.g. ether oxygen) that contributes to stronger coordination to Li<sup>+</sup> than TFSI oxygen. [68, 69]

#### 3.3. Electrochemical stability window (ESW)

NMC622 cathodes (or derivatives thereof) are considered promising for high energy battery applications regardless of their relatively complex surface chemistry that might be controlled by coatings, additives or other oxidatively robust electrolyte constituents upon cell operation. <sup>[70]</sup> Linear sweep voltammetry (LSV) conducted with inert electrodes of platinum and copper at an elevated temperature of 60 °C was employed to explore a more critical voltage range and relevant features of the introduced polymer electrolytes under the response of thermally accelerated decompositions (**Figure 2e**). <sup>[71, 72]</sup> Nevertheless, unlike a "dry" polymer of PTMC-grafted CDs where oxidative decomposition occurs solely at potentials above 5 V vs. Li|Li<sup>+</sup> (Figure S8, Supporting Information), <sup>[73]</sup> the quasi-solid electrolytes (e.g. 3A\_70PC) exhibit a reasonably high oxidative stability (~4.3 V vs. Li|Li<sup>+</sup>) owing to the presence of PC, in which sacrificial gas evolution (e.g. CO and CO<sub>2</sub>) could be accelerated at elevated temperatures and

likely occurs at lower potential, comparable to the proposed mechanistic details of ethylene carbonate (EC) oxidation. [72, 74-76] On the other side of the measurement, electrolytes of 3A 70PC behave quite stable during the cathodic scan, at least until potentials of -0.05 V vs. Li|Li<sup>+</sup> where Li plating begins. However, the experiments were performed with inert working electrodes that may overestimate the electrochemical stability, e.g. due to "smoother" surface contacts utterly different from typical composite cathodes that feature porous surface structures and disparate chemical environments. Hence, a galvanostatic measurement with active materials (NMC622) was further performed to corroborate ESW characterization.<sup>[77]</sup> As shown in Figure 2f, since the set charge cut-off voltage of 5.0 V is not reached and a subsequent discharge reveals a significantly high specific capacity loss, continuous oxidation associated with a voltage plateau or maximum turning point where severe electrolyte decompositions start to occur is identified at 4.5 V for 1A 50PC and at 4.4 V in cases of 2A 60PC and 3A 70PC, respectively, [77] similar to the data from potentiodynamic methods. It is feasible to ascribe the observed electrochemical oxidation to CO/CO2 release which evolves from carbonate-based plasticizers undergoing the chemical reactions with the reactive lattice oxygen of NMC.<sup>[78]</sup> In principle, based on the available electrochemical stability data, the class of materials comprising PTMC-based electrolytes is suitable for applications with commonly utilized cathode materials of LiCoO<sub>2</sub> and LiFePO<sub>4</sub>, but also LiNi<sub>x</sub>Mn<sub>y</sub>Co<sub>z</sub>O<sub>2</sub> or LiNi<sub>x</sub>Co<sub>y</sub>Al<sub>z</sub>O<sub>2</sub>.

# 3.4. Stability against lithium metal and mechanical suppression of high surface area lithium deposits

The stability of the polymer electrolytes and of high surface area lithium deposition dynamics, as e.g. induced by heterogeneous lithium deposition, govern the achievable longevity of considered cells. Both behaviors were allowed to be simply monitored based on the cycling performances in lithium symmetric cells with the introduced electrolytes. As seen in **Figure 3**a,

the Ohmic drop corresponds to both electrolyte and interfacial/interphasial resistances, while polarization effects are attributed to concentration gradients throughout the cells.<sup>[79, 80]</sup> Notably, the corresponding overvoltage in the case of 2A 60PC and 3A 70PC is smaller than for 1A 50PC and even reduces (<0.06 V) upon cycling, potentially due to more robust and denser solid electrolyte interphase (SEI) formation. In particular, the electrolyte 3A 70PC with highest cross-linking density tends to achieve an equilibration of (local) concentration gradients faster, thus reduced cell polarization (Figure S9a, Supporting Information). Contemporary studies have identified benefits of cross-linked polymers, [81] but established electrochemical stabilities and lithium deposition morphologies were not yet systematically compared among materials with variable cross-linking densities (Scheme 1). In an attempt to receive a remarkable difference on the deposited lithium surface, single-side galvanostatic plating with a high current density of 0.2 mA cm<sup>-2</sup> was applied for 10 h at 20 °C (Figure 3b); 1A 50PC could not withstand cycling at 0.2 mA cm<sup>-2</sup> as evidenced by the pronounced electrolyte decomposition, reaching a cut-off voltage of 1.5 V within 1.1 h, whereas the minor overvoltage (~0.1 V) present in case of 3A 70PC was anticipated owing to a formation of more compatible interphases and slightly higher lithium-ion conductivity (Figure 2). Overall, achieving higher cross-linking density is considered favorable to establish relatively more homogeneous lithium deposition when operating the introduced PTMC-based polymer electrolytes. The cells after a duration of 10 h single-side lithium plating were disassembled to explore the corresponding surface morphologies of the lithium electrodes (plating-side) and polymer membranes via SEM. The images display that only a few minor nuclei of lithium deposits are recognizable on the surface of plated electrode in the case of 1A 50PC (Figure S9b, Supporting Information) likely due to the earlier executive termination caused by the sample decomposition after ~1 h plating (Figure 3b), whereas surface morphologies of deposited lithium for the materials 2A 60PC and 3A 70PC appear quite distinct from the electrodes in contact with commercially employed liquid electrolytes (Figure 3c-f), where needle-like lithium deposits are often seen.<sup>[82]</sup> The "shape" of lithium deposits observed for 2A\_60PC exhibits more "angular", while "rounder" or "granular" structures are identified in case of 3A 70PC.

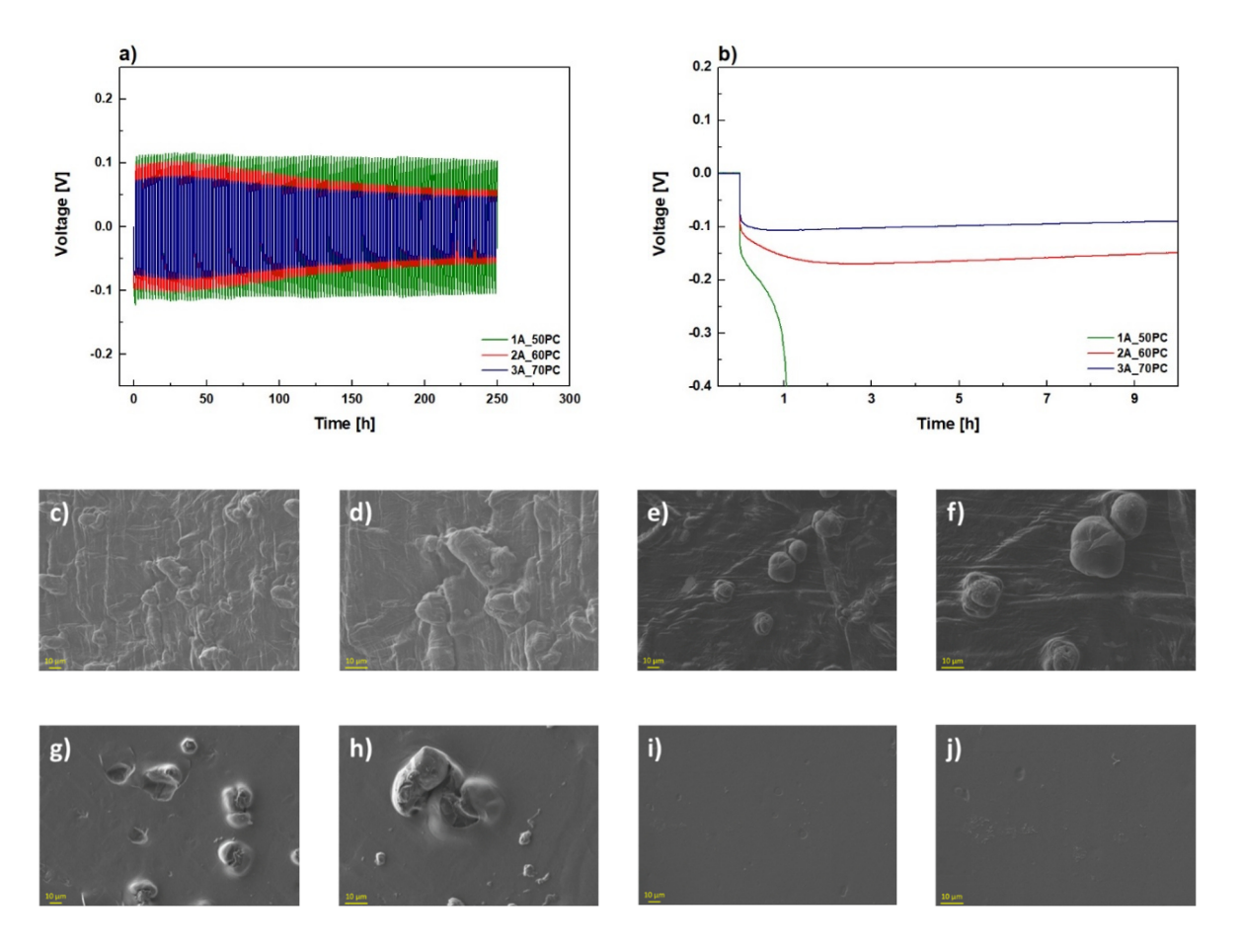


**Figure 3.** a) Lithium stripping/plating performance of the materials 1A\_50PC, 2A\_60PC and 3A\_70PC upon cycling at current density of 0.1 mA cm<sup>-2</sup> at 20 °C (1 h per half cycle). b) Voltage profiles of the presented materials after single-side lithium plating at 0.2 mA cm<sup>-2</sup> for 10 h (0.6 mg deposited lithium) at 20 °C in symmetric lithium cells. SEM images of plated lithium surfaces in the cases of c, d) 2A\_60PC and e, f) 3A\_70PC. Images of g, h) 2A\_60PC and i, j) 3A\_70PC membrane after 10 h single-side plating at a current density of 0.2 mA cm<sup>-2</sup> at 20 °C.

Upon inspection of the corresponding polymer membranes to comprehensively determine any impact of lithium deposition including membrane penetration, localized lithium deposits that partially insert into the electrolyte membrane of 2A\_60PC (**Figure 3**g,h) are evident, and some parts of the membrane are even pierced, likely due to limited mechanical stability (shown in **Figure 4**a,b). By contrast, membranes of 3A\_70PC (higher cross-linking density) exhibit adequate mechanical resistance, withstanding growing forces of localized lithium deposits (**Figure 3**i,j), though a few indistinct traces of deposited lithium appear on the membrane surfaces. This observation is in good agreement with rheological data that emphasize better

mechanical features in case of polymer membranes with higher cross-linking densities (**Figure** 4a).

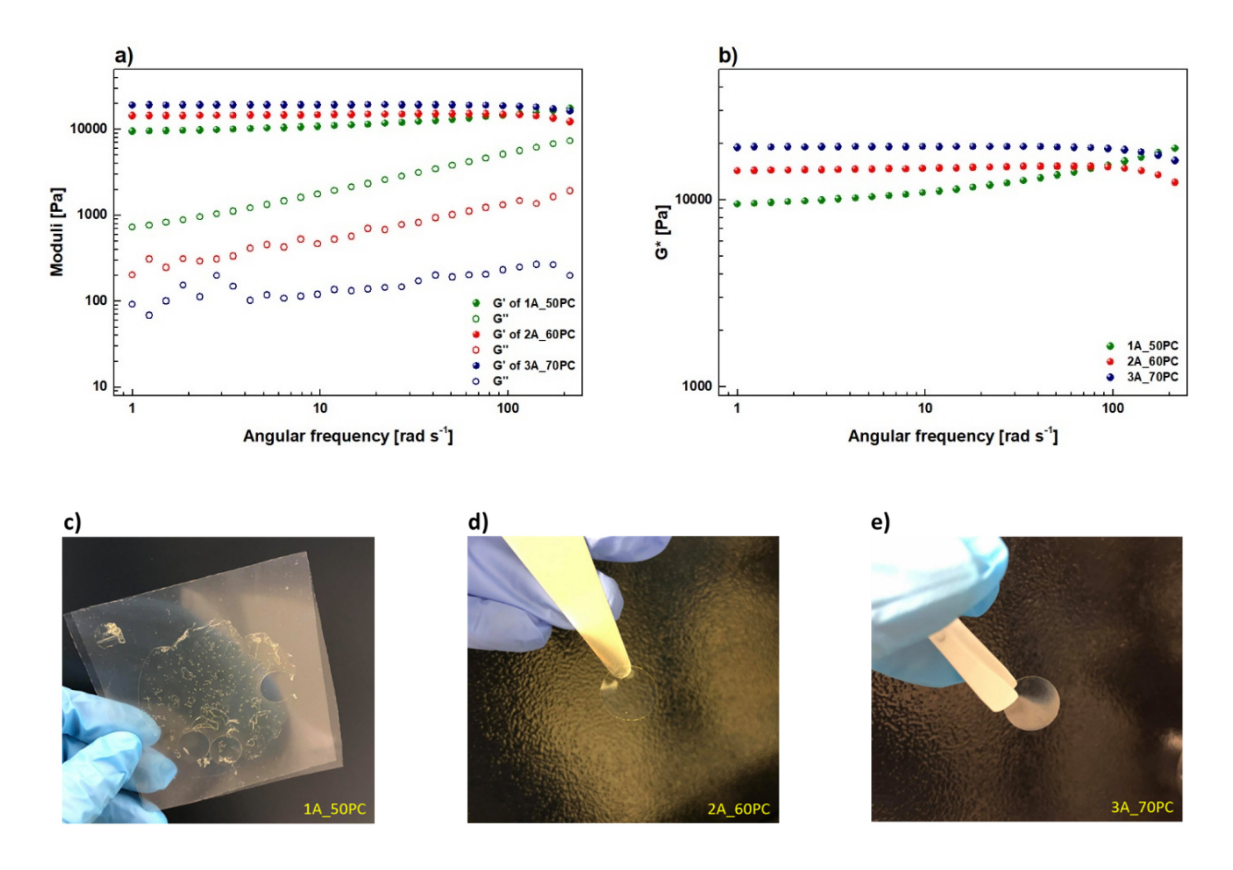


**Figure 4.** a) Storage, loss and b) complex moduli of materials 1A\_50PC, 2A\_60PC and 3A\_70PC at 20 °C. c-e) Membrane "appearances" of 1A\_50PC, 2A\_60PC and 3A\_70PC, respectively.

Despite that the overall mechanical strength (20 kPa) is much lower than the moduli of both lithium metal (6 GPa) and PEO (MPa range for mossy lithium depositions),<sup>[5]</sup> the introduced PTMC-based polymer electrolyte (3A\_70PC) effectively affords morphology control of lithium deposits, sufficiently hindering polymer penetration by localized lithium deposits, at least at the considered conditions. In addition, all polymer electrolytes (after reinforcement by crosslinking) act as elastic solids (that is, G' storage modulus > G'' loss modulus) at temperatures of 20 °C (**Figure 4**b) and 60 °C (Figure S10, Supporting Information).<sup>[16]</sup> Note that the 'qualities' of the membranes at variable degrees of cross-linking are visibly distinguishable, of which particularly 1A\_50PC features "curly" edges and some bubbles, likely reflecting the highly viscous precursor (**Figure 4**c-e). Consequently, the mechanical properties of polymer

electrolytes play an important role not only for avoiding high surface area lithium deposits but also for industrial membrane processing in view of e.g. polymer extrusion as common means.

# 3.5. Electrochemical performance in NMC622||Li cells and limiting current density

On the basis of the ESW data of this class of materials, NMC622 cathodes were selected for determining the long-term cycling performance while approaching demands of high-power applications. As shown in Figure 5a, the cycling stability of 1A 50PC (green) with the lowest cross-linking density is deficient, since after the 70<sup>th</sup> cycle the specific capacity significantly drops, reflecting severe decompositions and insufficient mechanical properties for suppressing inhomogeneous lithium deposits (Figure 4a-c). The electrolyte 2A 60PC (red) displays stable cycling behavior until the 207<sup>th</sup> cycle where short circuits appear afterwards, in good agreement with the SEM images indicating that the membrane could be ultimately pierced by localized lithium deposits (Figure 3h). By contrast, 3A 70PC (dark blue) with highest cross-linking density reveals superior cycling performance, affording 93.3% capacity retention (155.7 mAh g<sup>-1</sup>) and Coulombic efficiency of 99.7% after 300 cycles at 0.2C and 20 °C after the formation step (Figure S11, Supporting Information). Upon comparison of significant capacity losses in case of 2A 60PC (red), polymer 3A 70PC (dark blue) reflects relatively steady behavior and less capacity fade (see in Figure 5b). Generally, this class of materials with higher cross-linking densities (2A and 3A) appeared favorable to achieve long-term cycling stability; besides, the results of limiting current density disclose the potential of these electrolyte materials to go for rapid cycling (e.g. at rates of 2C or higher, as requested for electric vehicle applications) at elevated temperatures (displayed in Figure 5c,d).

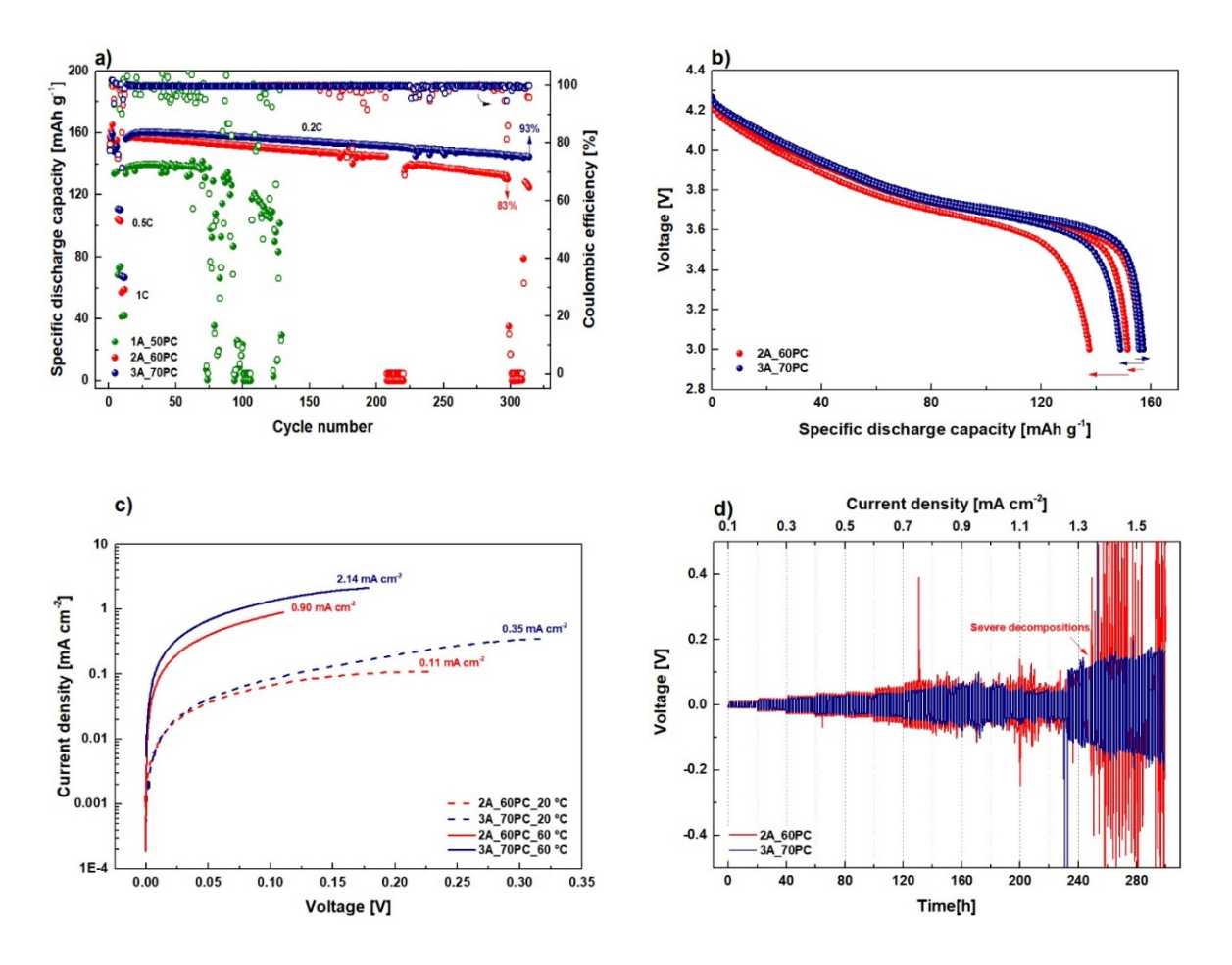


**Figure 5.** a) Long-term cycling performance of  $1A\_50PC$ ,  $2A\_60PC$  and  $3A\_70PC$  in NMC622||Li at 20 °C at a rate of 0.2C after a C-rate test as the formation step (0.05C/0.1C/0.2C/0.5C/1C, 3 cycles for each rate). b) Discharge voltage profiles of  $2A\_60PC$  and  $3A\_70PC$  at  $13^{th}$ ,  $100^{th}$  and  $250^{th}$  cycle. c) Determination of limiting current density of polymer  $2A\_60PC$  and  $3A\_70PC$  by linear sweep voltammetry in Li||Li cells at 20 °C and 60 °C, respectively. d) Lithium stripping and plating under different current densities (ranging from 0.1 to 1.5 mA cm<sup>-2</sup>, 10 cycles at each current density with 1h for every half cycle) at 60 °C.

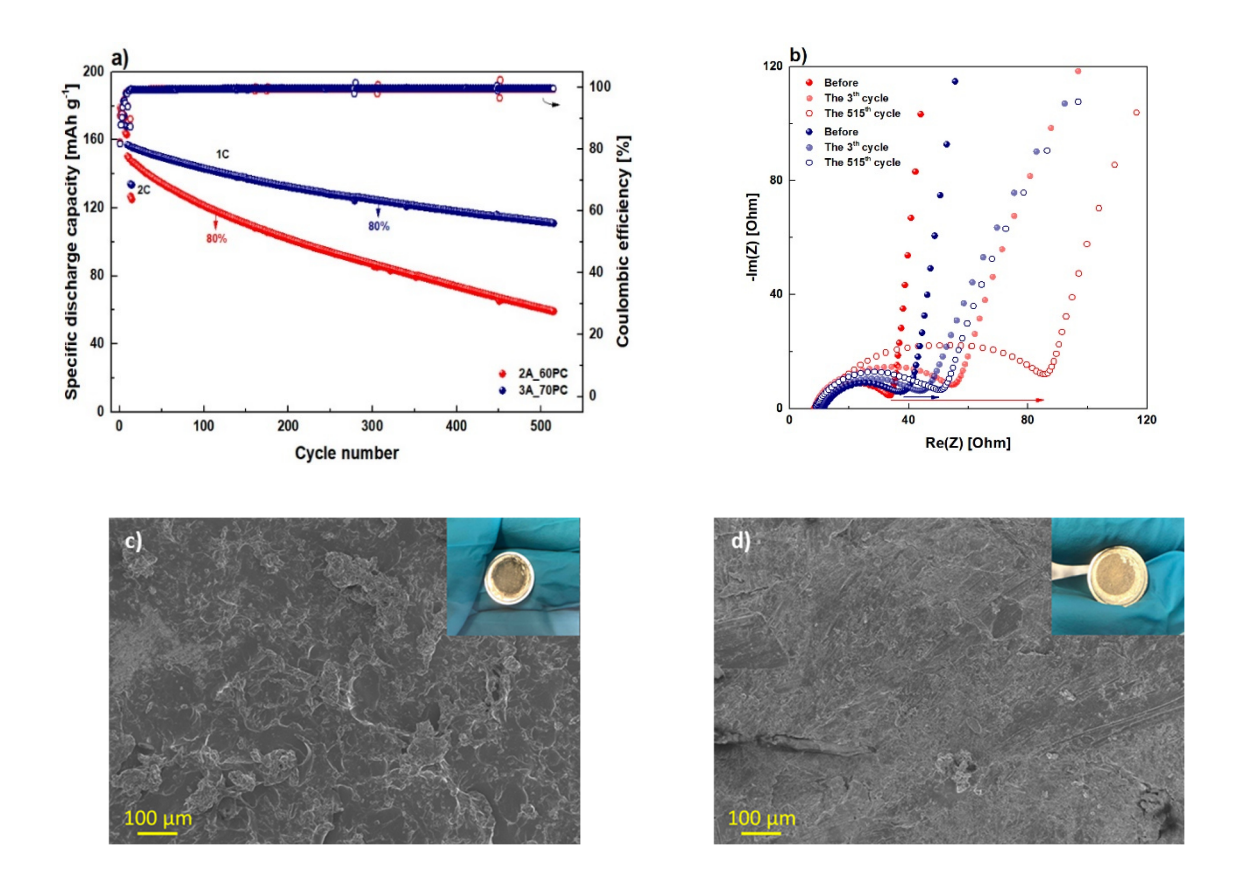
The limiting current density comprises an essential parameter to describe mass transfer limited by ion transport within electrolytes and diffusion through boundary layers typically present at membrane surfaces.<sup>[83]</sup> It is often invoked to indicate anticipated onsets of ion concentration gradients due to electrolyte diffusion limits that eventually leads to high surface area lithium deposits, e.g. by reason of localized anion depletion in the vicinity of the electrode;<sup>[5]</sup> however, it's not so regularly provided in other studies listed in **Scheme 1**, and the range of tested current density is mostly <1.0 mA cm<sup>-2</sup>. As illustrated in **Figure 5**c, the limiting current region is temperature dependent and increases at higher temperature (Figure S12, Supporting Information). The polymer 3A\_70PC appears to have enhanced tolerance to high current

density conditions (2.1 mA cm<sup>-2</sup> at 60 °C) compared to 2A\_60PC (0.9 mA cm<sup>-2</sup> at 60 °C), which may be indicative of relatively stable interphases and slightly higher lithium-ion mobility (see in **Figure 2**b,c and **Table 1**). Stripping/plating experiments at different current densities (shown in **Figure 5**d) also demonstrate that 2A\_60PC may behave fairly instable at high current densities, exhibiting irregularities at current density of 0.8 mA cm<sup>-2</sup> and severe electrolyte decompositions at current densities above 1.3 mA cm<sup>-2</sup>, finally evidencing micro-short circuits at 1.5 mA cm<sup>-2</sup>. On the contrary, short circuits are absent when utilizing the polymer electrolyte 3A\_70PC; the corresponding cycling performance is rather stable at least up to a current density of 1.5 mA cm<sup>-2</sup>. In summary, despite tolerating different limiting current densities, both polymers are suitable candidates to reasonably operate at higher C-rates (1C equals 0.4 mA cm<sup>-2</sup>) and elevated temperatures, where especially polymer electrolyte 3A\_70PC is applicable for faster charge conditions.

#### 3.6. Cycling behavior under high charge/discharge rates

In view of demands from rapidly expanding markets, a battery that can be charged/discharged in a short time attracts great attention. Therefore, fast charge/discharge cycling performance were evaluated at elevated temperatures to explore the long-term stability and establish the corresponding impacts of the cross-linking density. As shown in **Figure 6**a, both polymers provide sufficient specific discharge capacities (~150 mAh g<sup>-1</sup>) in NMC622||Li cells, offering high Coulombic efficiency (>99.3%) upon cycling at 1C and 60 °C, and no short circuits are observed within 500 cycles. However, cells with electrolyte 2A\_60PC suffer from a strong capacity decay during cycling, eventually attributed to parasitic side reactions (e.g. electrolyte decompositions, as reflected by higher impedances, **Figure 6**b), reaching a capacity retention (146.9 mAh g<sup>-1</sup>) of 80% at the 116<sup>th</sup> cycle. Cell longevity is better when using electrolytes with higher cross-linking density (e.g. 3A\_70PC), even achieving 80% capacity retention (155.4)

mAh g<sup>-1</sup>) at the 307<sup>th</sup> cycle. The impedance plots illustrate that interfacial/interphasial resistances in case of polymer 3A\_70PC increase less pronouncedly compared to polymer 2A\_60PC while the operation (**Figure 6**b), illustrating rather robust SEI formation and lesser electrolyte decomposition upon cycling. Moreover, the SEM images after long-term cycling reveal that the surfaces of lithium metal electrodes harvested from both cells have 2D planar lithium deposits (**Figure 6**c,d). Particularly in the case of 3A\_70PC, the lithium deposit morphology appears smooth and dense, likely reflecting robust SEI layer formation and enhanced mechanical properties, thereby sufficiently suppressing high surface area lithium deposits. The ability of solvent entrapment is controlled by the actual cross-linking density (**Figure 2**d), as supported by the noticeable liquid phase leaking and reactions with Al current collectors at the back side of cathode found in the case of disassembled cells operated with 2A\_60PC and after long-term cycling at 60 °C (Figure S13, Supporting Information), while it is indeed not the case when utilizing 3A 70PC.



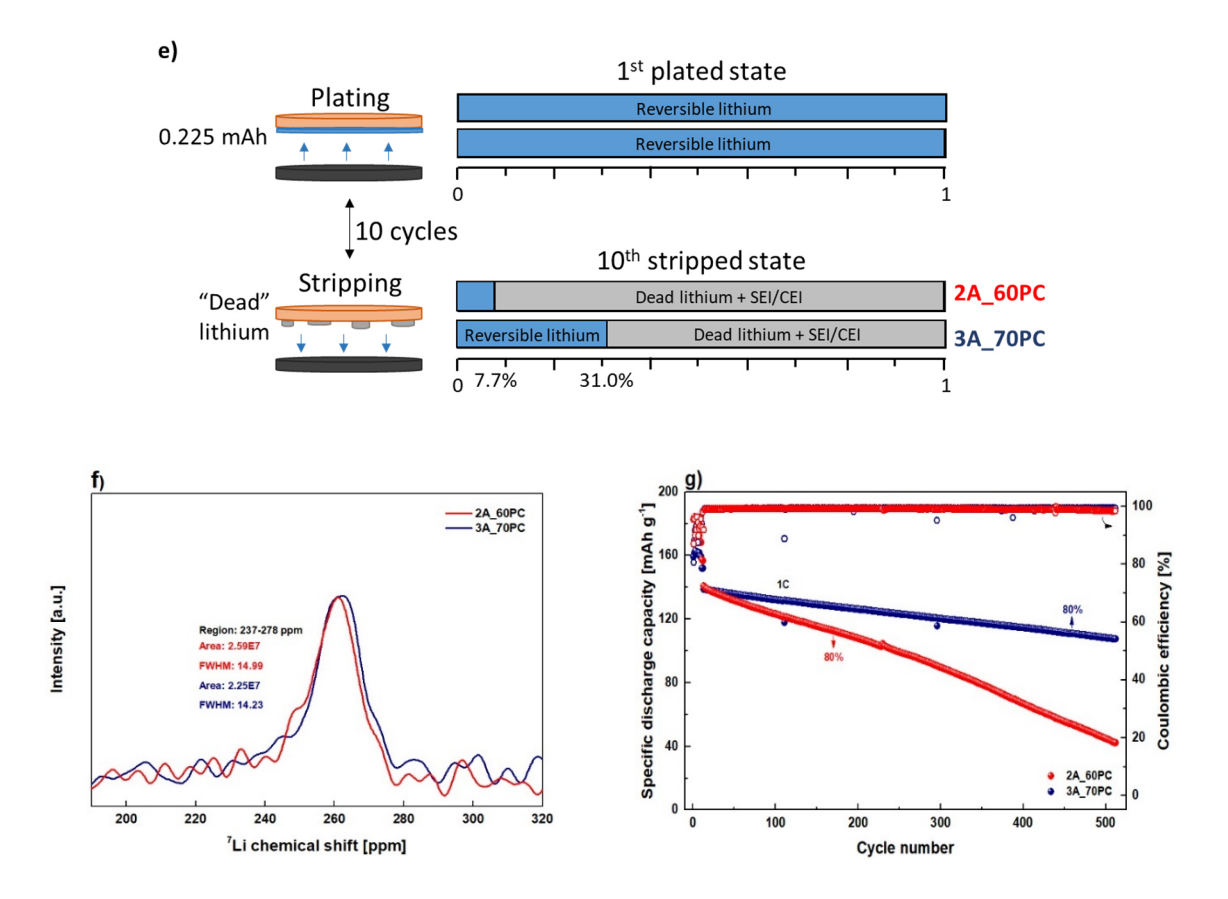


**Figure 6.** a) Long-term cycling performance of polymers 2A\_60PC and 3A\_70PC with 1C at 60 °C after the formation step (0.1C/0.2C/0.5C/1C/2C, 3 cycles at each rate). b) Impedance plots of polymers 2A\_60PC (red) and 3A\_70PC (blue) before and after the formation step at 0.1C for 3 cycles at 60 °C. SEM images of lithium surfaces from the full cells of c) 2A\_60PC and d) 3A\_70PC after 500 cycles with 1C at 60 °C. e) Schematic representation of contributions to lithium species and f) exsitu <sup>7</sup>Li solid-state NMR spectra of anode-free cells with polymer electrolytes of 2A\_60PC and 3A\_70PC after operation at 1C and 60 °C for 10 cycles. g) Long-term cycling performance of polymers 2A\_60PC and 3A\_70PC with 1C at 40 °C after a formation step (0.05C/0.1C/0.05C/0.1C/0.2C/0.5C/1C, 2 cycles for each rate).

An "anode-free" system (copper foil as anode substrate with "zero-excess lithium") is also explored to closely monitor the morphology of lithium deposits and compare fractions of "dead lithium" in both electrolytes based on a recently introduced protocol invoking (ex-situ) <sup>7</sup>Li solid-state NMR.<sup>[84]</sup> Typically, significant capacity losses are observed in this cell configuration, due to rather inhomogeneous lithium deposits and a limited reservoir of active lithium available from the cathode. The latter is even further reduced upon cycling based on gradual consumption by SEI and CEI (cathode electrolyte interphase)<sup>[85]</sup> formation or occurring "dead lithium" fractions.<sup>[40, 86]</sup> After 10 cycles (Figure S14a, Supporting Information), the corresponding fractions of reversible lithium amount to 7.7% and 31.0% (~0.225 mAh capacity at 1<sup>st</sup>

charged/plated state) in the cells with polymers 2A 60PC and 3A 70PC, respectively (Figure 6e), revealing that most of the active lithium is already depleted by the formation of "dead lithium" and electrolyte decomposition at the interphases. On the basis of their characteristic <sup>7</sup>Li NMR chemical shifts, microstructures of deposited lithium are readily distinguished as "dendritic" (270 ppm), "mossy" (260 ppm) or "smooth" (245 ppm) deposits. [84] As displayed in Figure 6f, the total amount of "dead lithium" is somewhat pronounced in case of polymers with lower cross-linking density, though the actual differences between the considered electrolytes are not so significant to fully interpret the strong capacity drop in case of 2A 60PC, thus implying that parasitic side reactions (e.g. electrolyte decomposition and SEI formation) substantially impact on the reversible lithium consumptions, eventually resulting in low Coulombic efficiency. Note that the actual fractions of "dead lithium" (lithium deposits) in case of both materials exhibit "mossy" microstructures, since the highest <sup>7</sup>Li NMR signal of deposited lithium appears at 261-262 ppm. Furthermore, the deconvoluted NMR spectra accounting for the presence of up to three distinct lithium metal species indicate less amounts of "dendritic" lithium in cells of 3A 70PC (Figure S14b and Table S3, Supporting Information), consistent with the SEM data of lithium surfaces after cycling of the polymer electrolytes in NMC622||Li cells (Figure 6c,d).

Parasitic side reactions have strong impact on the achievable cell longevity and may be accelerated at higher temperatures, possibly fostering faster decay of the reversible specific capacity. Hence, cell operations were also adjusted to a moderate temperature of 40 °C. Indeed, cycling stability of the cells are pronouncedly improved, featuring reduced capacity losses upon cycling (**Figure 6**g and Figure S15a, Supporting Information). Despite the fact that the available specific discharge capacity is slightly decreased (~140 mAh g<sup>-1</sup>, at 1C) at this moderate temperature in both electrolytes, the polymer 2A\_60PC as well as 3A\_70PC afford better capacity retention at the 170<sup>th</sup> and 457<sup>th</sup> cycle where capacity retention remains at 80% as compared to the operations at 60 °C (Figure S15b, Supporting Information). Additionally, the

data are in good agreement with previous results, certainly illustrating that polymers with higher cross-linking density exhibit superior stability and electrochemical performance with respect to long-term cycling. Overall, the temperature significantly affects the cycling behavior and cell stability, likely due to detrimental side reactions occurring upon cycling at higher temperatures.

#### 3.7. LiNbO<sub>3</sub> coated NMC622 cathode

To date, available cathode coating technologies are continuously refined. As protective layer on top of active materials, such coatings allow to inhibit or mitigate detrimental side reactions otherwise occurring at cathode surfaces in contact with electrolytes, thereby fostering prolonged cell life. Herein, NMC622 with thin LiNbO3 coating layer is employed to effectively improve the cycling performance of the polymers at 60°C. In **Figure 7**a, the data at 1C clearly emphasize that cycling stability of NMC622||Li cells in the presence of coated NMC622 is significantly enhanced (Figure S15c, Supporting Information), affording over a hundred cycles more compared to "pristine" cathode materials prior to reaching the cut-off capacity (state of health, SOH 80%) at 60 °C, indicating fewer fractions of electrolyte decomposition occurring upon cycling, likely because of "indirect" contact with NMC active materials, similar to the effective concept of carbon coating exploited in case of LFP. [44, 87] This is corroborated by impedance plots (**Figure 7**b) where interfacial/interphasial resistances in the presence of coated NMC622 are smaller compared to "pristine" NMC after cycling and even decrease upon cycling, reflecting more robust interphases.

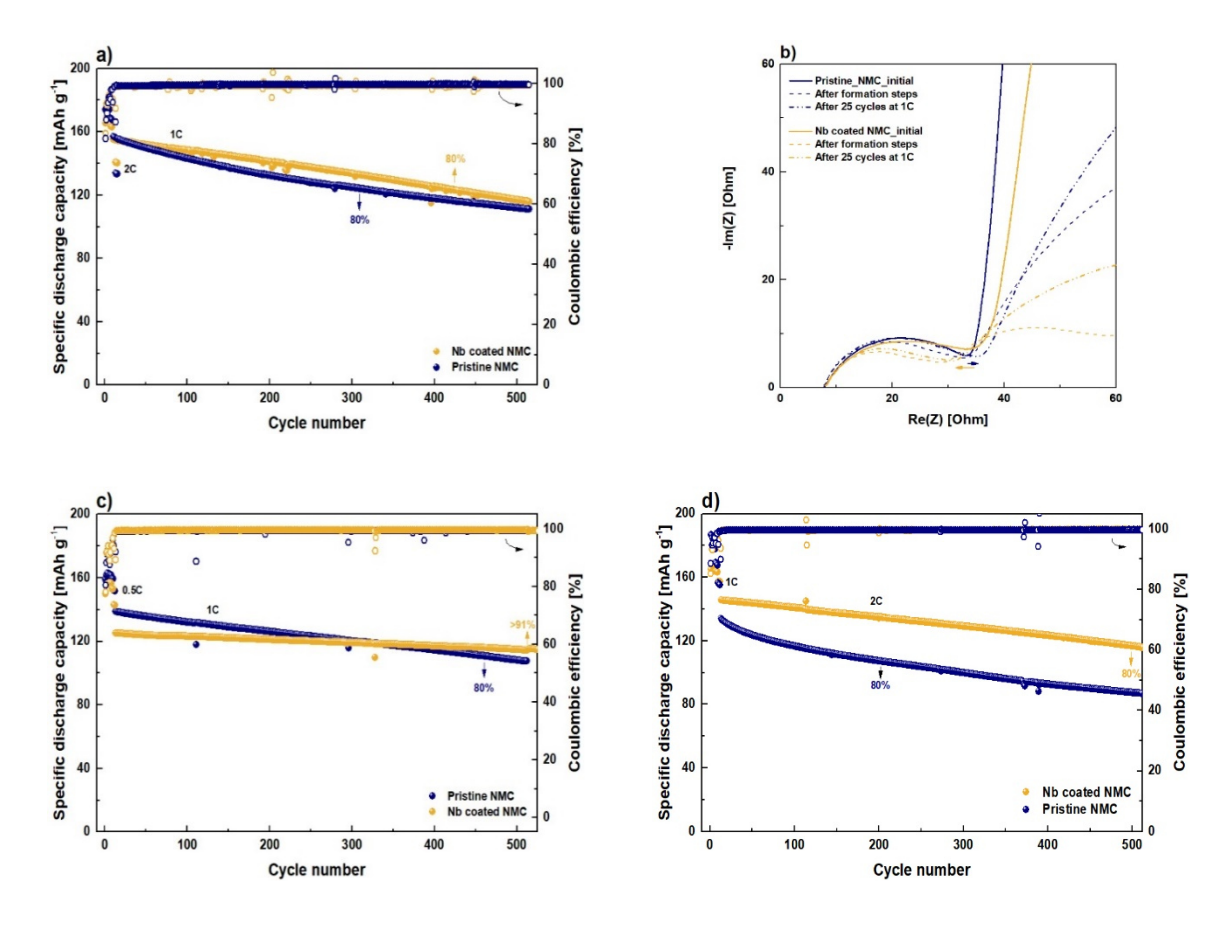


Figure 7. The comparison of long-term cycling performance data at 1C against with pristine NMC and LiNbO $_3$  coated NMC in presence of polymer electrolyte 3A\_70PC at a) 60 °C c) 40 °C. b) Impedance plots of polymers 3A\_70PC against pristine NMC and coated NMC before and after the formation step (0.1C/0.2C/0.5C/1C/2C, 3 cycles for each) and following 25 cycles with 1C at 60 °C d) Long-term cycling performances of polymers 3A\_70PC at 2C and 60 °C after a formation step (0.1C/0.2C/0.5C/1C/2C, 3 cycles for each rate).

A parallel trend is identified for cells running at 40 °C exhibiting more than 91% capacity retention (125.2 mAh g<sup>-1</sup>) after the 512<sup>th</sup> cycle at 1C (80% at the 903<sup>th</sup> cycle in Figure S16, Supporting Information) in spite of a slightly decreased discharge capacity, as anticipated for non-conductive coating layers that may negatively impact on charge carrier transport properties (**Figure 7**c).<sup>[42]</sup> Moreover, since the formation step shown in **Figure 7**a and Figure S15c (Supporting Information) reveals the potential of rapid charge/discharge at an even higher C-rate (2C) with reasonably high specific discharge capacity when exploiting coated NMC622, the long-term electrochemical behavior upon cycling at 2C is also explored, displaying a higher capacity of 145.7 mAh g<sup>-1</sup> and very promising capacity retention of 80% at the 504<sup>th</sup> cycle in comparison to pristine NMC622 that retains SOH 80% only at the 201<sup>th</sup> cycle (**Figure 7**d). In

principle, these results successfully demonstrate the applicability of the introduced polymer materials when cycled in the presence of suitably coated active materials, rendering them highly promising "quasi-solid" electrolytes.

#### 4. Conclusion

Towards achieving solid-state high energy density batteries, the technology of exploiting "quasi-solid" electrolytes (employing small amounts of liquid phase that could be effectively entrapped) keeps a step ahead of conventional gel systems. Notably, the introduced PTMCbased "quasi-solid" electrolytes with fine-tuned cross-linking densities feature rather robust electrochemical performance, offering superior cycling stability and less degrees of electrolyte decomposition upon operations in NMC622||Li cells. In general, considering that fast charging and discharging of battery cells comprise a key to determine prospects of practical applications, all presented materials successfully demonstrate rapid cycling at rates of 1C and 2C, respectively, at both 40 and 60 °C, exhibiting prominent capacity retention (91% and 80% SOH after 500 cycles) and extended longevity, clearly reflecting benefits from protective coatings on cathode active materials (LiNbO<sub>3</sub> coated NMC622). In summary, the obtained results clearly highlight that systematic adjustment of cross-linking densities of polymer electrolytes and exploitation of both suitable coatings on active materials as well as molecular entrapment of plasticizers constitute a highly viable concept not only to boost salient features of polymer electrolytes but also to substantially prolong cell lifetimes, which thus represents an expedient approach for materials development towards eventually achieving solid polymer-electrolytebased cells.

## Glossary

List of definitions and acronyms of field-specific terms

Acronym	Meaning	
α	Ion dissociation degree	
CD	Cyclodextrin	
CEI	Cathode electrolyte interphase	
DBU	1,8-Diazabicyclo [5.4.0] undec-7-ene	
DCC	N,N'-Dicyclohexylcarbodiimide	
DMAc	Dimethylacetamide	
DMAP	4-(Dimethylamino)pyridine	
DMPA	2,2-Dimethoxy-2-phenylacetophenone	
DMSO	Dimethyl sulfoxide	
DSC	Differential scanning calorimetry	
EC	Ethylene carbonate	
EIS	Electrochemical impedance spectroscopy	
EOEOEA	2-(2-Ethoxyethoxy) ethyl acrylate	
ESW	Electrochemical stability window	
FAME	mono-Ethyl fumarate	
G', G''	Storage modulus, loss modulus	
GCD	Grafted cyclodextrin	
GPC	Gel permeation chromatography	
GPR	Grafted polyrotaxane	
HSAL	High surface area lithium	
LFP	Lithium iron phosphate	
LIB	Lithium-ion battery	
LiTFSI	Lithium bis-trifluoro-methane-sulfonimide	
LMB	Lithium metal battery	
LSV	Linear sweep voltammetry	
NMC	Lithium nickel manganese cobalt	
NMR	Nuclear magnetic resonance	
NMP	N-methyl-2-pyrrolidone	
ОСР	Open circuit potential	
PC	Propylene carbonate	
PE	Polymer electrolyte	
PEO	Polyethylene oxide	
PFG	Pulsed field gradient	
PMMA	Poly(methyl methacrylate)	
PTMC	Poly(trimethylene carbonate)	
PVdF	polyvinylidene difluoride	
ROP	Ring-opening polymerization	
RT	Room temperature	
SEI	Solid electrolyte interphase	
SEM	Scanning electron microscopy	
σLi+	Lithium-ion conductivity	

SOH	State of health
SPE	Solid polymer electrolyte
SSE	Solid-state electrolyte
t <sub>+</sub>	Transference number

# Acknowledgments

The authors M.C., M.W., and G.B. gratefully acknowledge generous support by the German Federal Ministry of Education and Research (BMBF) within 'Festbatt' (polymer platform, grant: 13XP0175A). Special thanks to Philipp Röring for cathode preparation, Susanna Krämer for measuring DSC data, Yi-Chen Hsieh for SEM operation, Dr. Jaschar Atik and Dr. Annika Buchheit for the assistances on rheology analysis and the determination of transference numbers, respectively. The authors thank Dr. Fabian Kempe for fruitful discussions of the manuscript.

#### References

- [1] A. Kolesnikov, M. Kolek, J. F. Dohmann, F. Horsthemke, M. Börner, P. Bieker, M. Winter, M. C. Stan, *Adv. Energy Mater.* **2020**, *10*, 2000017.
- [2] V. Küpers, M. Kolek, P. Bieker, M. Winter, G. Brunklaus, *Phys. Chem. Chem. Phys.*2019, 21, 26084.
- [3] P. Lennartz, K. Borzutzki, M. Winter, G. Brunklaus, *Electrochim. Acta* **2021**, *388*, 138526.
- [4] J. R. Nair, L. Imholt, G. Brunklaus, M. Winter, *The Electrochemical Society Interface* **2019**, *28*, 55.
- [5] P. Barai, K. Higa, V. Srinivasan, *Phys. Chem. Chem. Phys.* **2017**, *19*, 20493.
- [6] L. Fan, S. Wei, S. Li, Q. Li, Y. Lu, Adv. Energy Mater. 2018, 8, 1702657.
- [7] C. Monroe, J. Newman, *J. Electrochem. Soc.* **2005**, *152*, A396.

- [8] W. Zhao, J. Yi, P. He, H. Zhou, *EER* **2019**, *2*, 574.
- [9] M. S. Grewal, M. Tanaka, H. Kawakami, *Polym. Int.* **2019**, *68*, 684.
- [10] Q. Pan, D. Barbash, D. M. Smith, H. Qi, S. E. Gleeson, C. Y. Li, *Adv. Energy Mater*.2017, 7, 1701231.
- [11] H. Wang, Q. Wang, X. Cao, Y. He, K. Wu, J. Yang, H. Zhou, W. Liu, X. Sun, *Adv. Mater.* **2020**, *32*, 2001259.
- [12] J. Shi, Y. Yang, H. Shao, J. Membr. Sci. 2018, 547, 1.
- [13] K. Borzutzki, J. Thienenkamp, M. Diehl, M. Winter, G. Brunklaus, *J. Mater. Chem. A* **2019**, 7, 188.
- [14] H.-D. Nguyen, G.-T. Kim, J. Shi, E. Paillard, P. Judeinstein, S. Lyonnard, D. Bresser,C. Iojoiu, *Energy Environ. Sci.* 2018, 11, 3298.
- [15] H.-x. Xie, Q.-g. Fu, Z. Li, S. Chen, J.-m. Wu, L. Wei, X. Guo, Chem. Eur. J. 2021, 27, 7773.
- [16] D.-M. Shin, J. E. Bachman, M. K. Taylor, J. Kamcev, J. G. Park, M. E. Ziebel, E. Velasquez, N. N. Jarenwattananon, G. K. Sethi, Y. Cui, J. R. Long, *Adv. Mater.* 2020, 32, 1905771.
- [17] A. Concheiro, C. Alvarez-Lorenzo, Adv. Drug Del. Rev. 2013, 65, 1188.
- [18] H. A. Panahi, H. S. Alaei, Int. J. Pharm. 2014, 476, 178.
- [19] L. Imholt, D. Dong, D. Bedrov, I. Cekic-Laskovic, M. Winter, G. Brunklaus, ACS

  Macro Letters 2018, 7, 881.
- [20] L. Imholt, T. S. Dörr, P. Zhang, L. Ibing, I. Cekic-Laskovic, M. Winter, G. Brunklaus, J. Power Sources 2019, 409, 148.
- [21] K. Kato, K. Inoue, M. Kudo, K. Ito, Beilstein J. Org. Chem. 2014, 10, 2573.

- [22] J. Araki, T. Kataoka, K. Ito, Soft Matter 2008, 4, 245.
- [23] H. Ben youcef, O. Garcia-Calvo, N. Lago, S. Devaraj, M. Armand, *Electrochim. Acta* **2016**, *220*, 587.
- [24] V. Chaudoy, F. Ghamouss, E. Luais, F. Tran-Van, *Ind. Eng. Chem. Res.* **2016**, *55*, 9925.
- [25] S. Park, B. Jeong, D.-A. Lim, C. H. Lee, K. H. Ahn, J. H. Lee, D.-W. Kim, ACS Appl. Mater. Interfaces 2020, 12, 19553.
- [26] M. Řezanka, Environ. Chem. Lett. 2019, 17, 49.
- [27] W. Ding, C. Wei, S. Wang, L. Zou, Y. Gong, Y. Liu, L. Zang, *Polymers* **2019**, *11*, 1296.
- [28] S. Jankowsky, M. M. Hiller, R. Stolina, H. D. Wiemhöfer, *J. Power Sources* **2015**, *273*, 574.
- [29] R. He, T. Kyu, *Macromolecules* **2016**, *49*, 5637.
- [30] Q. Xiao, C. Deng, Q. Wang, Q. Zhang, Y. Yue, S. Ren, ACS Omega 2019, 4, 95.
- [31] Q. Lu, J. Fang, J. Yang, R. Miao, J. Wang, Y. Nuli, J. Membr. Sci. 2014, 449, 176.
- [32] Q. Lu, J. Yang, W. Lu, J. Wang, Y. Nuli, *Electrochim. Acta* **2015**, *152*, 489.
- [33] R. Khurana, J. L. Schaefer, L. A. Archer, G. W. Coates, J. Am. Chem. Soc. 2014, 136, 7395.
- [34] C. Liao, X.-G. Sun, S. Dai, *Electrochim. Acta* **2013**, *87*, 889.
- [35] X. Zuo, X.-M. Liu, F. Cai, H. Yang, X.-D. Shen, G. Liu, *J. Power Sources* **2013**, *239*, 111.
- [36] Z. Chen, D. Steinle, H.-D. Nguyen, J.-K. Kim, A. Mayer, J. Shi, E. Paillard, C. Iojoiu,S. Passerini, D. Bresser, *Nano Energy* 2020, 77, 105129.
- [37] P. Sutton, M. Airoldi, L. Porcarelli, J. L. Olmedo-Martínez, C. Mugemana, N. Bruns,D. Mecerreyes, U. Steiner, I. Gunkel, *Polymers* 2020, *12*, 595.

- [38] S. S. Hwang, C. G. Cho, H. Kim, *Electrochem. Commun.* **2010**, *12*, 916.
- [39] X. Pan, H. Sun, Z. Wang, H. Huang, Q. Chang, J. Li, J. Gao, S. Wang, H. Xu, Y. Li, W. Zhou, Adv. Energy Mater. 2020, 10, 2002416.
- [40] J. Xiao, Q. Li, Y. Bi, M. Cai, B. Dunn, T. Glossmann, J. Liu, T. Osaka, R. Sugiura, B.Wu, J. Yang, J.-G. Zhang, M. S. Whittingham, *Nat. Energy* 2020, 5, 561.
- [41] M. J. Herzog, D. Esken, J. Janek, *Batter. Supercaps* **2021**, *n/a*.
- [42] H. Zhang, J. Xu, J. Zhang, Fron. Mater. 2019, 6.
- [43] M. Otoyama, Y. Ito, A. Hayashi, M. Tatsumisago, *Electrochem.* **2016**, *84*, 812.
- [44] A. Y. Kim, F. Strauss, T. Bartsch, J. H. Teo, T. Hatsukade, A. Mazilkin, J. Janek, P. Hartmann, T. Brezesinski, *Chem. Mater.* **2019**, *31*, 9664.
- [45] D. Becker, M. Börner, R. Nölle, M. Diehl, S. Klein, U. Rodehorst, R. Schmuch, M. Winter, T. Placke, ACS Appl. Mater. Interfaces 2019, 11 20, 18404.
- [46] S. Hildebrand, C. Vollmer, M. Winter, F. Schappacher, *J. Electrochem. Soc.* 2017, 164,A2190.
- [47] Q. Hou, D. W. Grijpma, J. Feijen, *Acta Biomater.* **2009**, *5*, 1543.
- [48] V. Mereacre, P. Stüble, A. Ghamlouche, J. R. Binder, *Nanomaterials* **2021**, *11*, 548.
- [49] P. W. Kuchel, G. Pagès, K. Nagashima, S. Velan, V. Vijayaragavan, V. Nagarajan, K.H. Chuang, Conc. Magn. Reson. A 2012, 40A, 205.
- [50] D. Sinnaeve, Conc. Magn. Reson. A 2012, 40A, 39.
- [51] A. Hosseinioun, P. Nürnberg, M. Schönhoff, D. Diddens, E. Paillard, RSC Adv. 2019,9, 27574.
- [52] M. Watanabe, S. Nagano, K. Sanui, N. Ogata, Solid State Ion. 1988, 28-30, 911.
- [53] Y. Kato, M. Watanabe, K. Sanui, N. Ogata, Solid State Ion. 1990, 40-41, 632.

- [54] A. Nishimoto, M. Watanabe, Y. Ikeda, S. Kohjiya, *Electrochim. Acta* **1998**, *43*, 1177.
- [55] M. Siekierski, M. Bukat, M. Ciosek, M. Piszcz, M. Mroczkowska-Szerszeń, *Polymers*2021, 13, 895.
- [56] K. D. Fong, J. Self, K. M. Diederichsen, B. M. Wood, B. D. McCloskey, K. A. Persson, ACS Cent. Sci. 2019, 5, 1250.
- [57] M. Grünebaum, M. M. Hiller, H. D. Wiemhöfer (WWU), DE 102013004204, 2014
- [58] R. Nölle, K. Beltrop, F. Holtstiege, J. Kasnatscheew, T. Placke, M. Winter, *Mater. Today* **2020**, *32*, 131.
- [59] J. Owen, Comprehensive Polymer Science and Supplements, 2 (Eds: G. Allen, J. C. Bevington), Pergamon, Amsterdam 1989, Ch. 21.
- [60] T. Sakakibara, M. Kitamura, T. Honma, H. Kohno, T. Uno, M. Kubo, N. Imanishi, Y. Takeda, T. Itoh, *Electrochim. Acta* 2019, 296, 1018.
- [61] L. Wang, J. Li, G. Lu, W. Li, Q. Tao, C. Shi, H. Jin, G. Chen, S. Wang, Fron. Mater.2020, 7.
- [62] E. R. Logan, J. R. Dahn, Trends Chem. 2020, 2, 354.
- [63] A. Ehrl, J. Landesfeind, W. A. Wall, H. A. Gasteiger, J. Electrochem. Soc. 2017, 164, A2716.
- [64] Z. Wang, W. Gao, X. Huang, Y. Mo, L. Chen, J. Raman Spectrosc. 2001, 32, 900.
- [65] M. Bergman, A. Bergfelt, B. Sun, T. Bowden, D. Brandell, P. Johansson, *Electrochim. Acta* **2015**, *175*, 96.
- [66] Y. Saito, K. Hirai, S. Murata, Y. Kishii, K. Kii, M. Yoshio, T. Kato, J. Phys. Chem. B2005, 109, 11563.
- [67] Y. Aihara, S. Arai, K. Hayamizu, *Electrochim. Acta* **2000**, *45*, 1321.

- [68] O. Borodin, G. D. Smith, *Macromolecules* **2006**, *39*, 1620.
- [69] D. Diddens, A. Heuer, O. Borodin, *Macromolecules* **2010**, *43*, 2028.
- [70] Y. Arinicheva, M. Wolff, S. Lobe, C. Dellen, D. Fattakhova-Rohlfing, O. Guillon, D. Boehm, F. Zoller, R. Schmuch, J. Li, M. Winter, E. Adamczyk, V. Pralong, *Advanced Ceramics for Energy Conversion and Storage*, in *Elsevier Series on Advanced Ceramic Materials* Vol. 746 (Eds: O. Guillon), M. Deans, 2020, Ch. 10.
- [71] G. T. Kim, G. B. Appetecchi, M. Carewska, M. Joost, A. Balducci, M. Winter, S. Passerini, *J. Power Sources* **2010**, *195*, 6130.
- [72] M. Metzger, P. Walke, S. Solchenbach, G. Salitra, D. Aurbach, H. A. Gasteiger, J. Electrochem. Soc. 2020, 167, 160522.
- [73] B. Sun, J. Mindemark, K. Edström, D. Brandell, Solid State Ion. 2014, 262, 738.
- [74] M. Metzger, B. Strehle, S. Solchenbach, H. A. Gasteiger, *J. Electrochem. Soc.* **2016**, *163*, A798.
- [75] M. Leißing, M. Winter, S. Wiemers-Meyer, S. Nowak, J. Chromatogr. A 2020, 1622, 461122.
- [76] J.-P. Schmiegel, M. Leißing, F. Weddeling, F. Horsthemke, J. Reiter, Q. Fan, S. Nowak,
   M. Winter, T. Placke, J. Electrochem. Soc. 2020, 167, 060516.
- [77] J. Kasnatscheew, B. Streipert, S. Röser, R. Wagner, I. Cekic Laskovic, M. Winter, *Phys. Chem. Chem. Phys.* **2017**, *19*, 16078.
- [78] R. Jung, M. Metzger, F. Maglia, C. Stinner, H. A. Gasteiger, *J. Electrochem. Soc.* **2017**, *164*, A1361.
- [79] G. M. A. Girard, X. Wang, R. Yunis, D. R. MacFarlane, A. J. Bhattacharyya, M. Forsyth,P. C. Howlett, *Batter. Supercaps* 2019, 2, 229.

- [80] M. Rosso, C. Brissot, A. Teyssot, M. Dollé, L. Sannier, J.-M. Tarascon, R. Bouchet, S. Lascaud, *Electrochim. Acta* 2006, 51, 5334.
- [81] Y. Ma, J. Ma, J. Chai, Z. Liu, G. Ding, G. Xu, H. Liu, B. Chen, X. Zhou, G. Cui, L. Chen, ACS Appl. Mater. Interfaces 2017, 9, 41462.
- [82] D. Rehnlund, C. Ihrfors, J. Maibach, L. Nyholm, *Mater. Today* **2018**, *21*, 1010.
- [83] V. M. Barragán, C. Ruíz-Bauzá, J. Colloid Interface Sci. 1998, 205, 365.
- [84] Y.-C. Hsieh, M. Leißing, S. Nowak, B.-J. Hwang, M. Winter, G. Brunklaus, *Cell Rep. Phys. Sci.* **2020**, *1*, 100139.
- [85] D. R. Gallus, R. Wagner, S. Wiemers-Meyer, M. Winter, I. Cekif Laskovic, Electrochim. Acta 2015, 184, 410.
- [86] Y.-C. Hsieh, J. H. Thienenkamp, C.-J. Huang, H.-C. Tao, U. Rodehorst, B. J. Hwang,
   M. Winter, G. Brunklaus, *The Journal of Physical Chemistry C* 2021, 125, 252.
- [87] Z.-X. Chi, W. Zhang, F.-Q. Cheng, J.-T. Chen, A.-M. Cao, L.-J. Wan, *RSC Adv.* **2014**, 4, 7795.